GRUMMAN AEROSPACE CORPORATION

RESEARCH & DEVELOPMENT CENTER

Second Year Final Report on NASA Contract NAS8-32998

REPORT RE-693

THE GROWTH OF METASTABLE PERITECTIC COMPOUNDS

DECEMBER 1984

prepared by

David J. Larson, Jr.
Materials and Structural Mechanics

Research and Development Center
Grumman Aerospace Corporation
Bethpage, New York 11714

prepared for

National Aeronautics and Space Administration
George C. Marshall Flight Center
Marshall Space Flight Center
Alabama 35812

Approved by: Richard A. Scheuing
Richard A. Scheuing, V.P.
Director, R&D Center

ABSTRACT

In this program, the influence of gravitationally driven convection on the directional solidification of peritectic alloys was evaluated. The Pb-Bi peritectic was studied as a model solidification system and results from this study will contribute to subsequent investigations of Co-Sm peritectic solidification.

Analyses of directionally solidified Pb-Bi peritectic samples indicate that appreciable macrosegregation occurs due to thermosolutal convection and/or Soret diffusion. The macrosegregation results in sequential change of phase and morphology as solidification progresses down the length of the sample, in accordance with equilibrium phase relationships and interface stability criteria.

Banding, reported earlier, was eliminated when furnace conditions were selected which resulted in a planar solidification interface. These conditions, presumably, led to a concomitant reduction in the convection driven by radial temperature gradients.

The directional solidification that occurs in the vicinity of the Pb-Bi peritectic isotherm has been found to be isocompositional and to consist solely of the equilibrium terminal solid solution and peritectic phases on an extremely fine scale. Evidence was found supporting the peritectic supercooling mechanism, however no evidence has been found to support the proposed peritectic superheat mechanism. In addition, this system cannot be described by the stagnant film model for two-phase equilibrium peritectic plane front solidification. Consequently, a new model is needed.

CONTENTS

ILLUSTRATIONS

Summary

1. INTRODUCTION

Many important materials solidify via a peritectic reaction. These include most cobalt-based superalloys, metal (M) - rare earth (RE) magnetic compounds (notably M_5RE and $M_{17}RE_2$), and A_3B superconductors. Single crystals or aligned two-phase composites are desirable morphologies for these materials. Current processing techniques have not produced aligned fibrous or lamellar two-phase composites, and single crystals have been grown only with great difficulty.

Plane-front directional solidification has been shown to produce aligned composite morphologies for eutectic, off-eutectic and monotectic solidification reactions. As a consequence, the directional solidification approach is an attractive candidate for processing peritectics. However, the anticipated peritectic two-phase composite microstructures have not been realized experimentally.

Chalmers (Ref. 1) was the first to anticipate the results that might be obtained from steady state, plane-front, directional solidification of peritectics. He assumed negligible diffusion in the solid and mixing in the liquid solely by diffusion. With respect to the peritectic reaction shown in Fig. 1 and for hypoperitectic alloys, i.e., $C_\alpha P < C_0 < C_\beta P$, Chalmers predicted a steady state consisting of simultaneous growth of α and β phases, producing a eutectic-like microstructure. Further, he predicted that hyperperitectic alloys ($C_\beta P < C_0 < C_L P$) would initially solidify α phase and the β phase would form when the liquid composition at the solidification interface reached $C_L P$.

Uhlmann and Chadwick (Ref. 2) were the first to directionally solidify hypoperitectic alloys to examine Chalmer's predictions. They observed that the steady state structures of all hypoperitectic alloys consisted of dendrites of the properitectic α phase in a matrix of peritectic β phase. However, the range of growth conditions was limited and Chalmers (Ref. 3) subsequently postulated that growth at higher ratios of thermal gradient to solidification velocity (G/V) might lead to cooperative growth, similar to that found in off-eutectic systems. This view was analytically supported by Livingston (Ref. 4) and Flemings (Ref. 5).

Boettinger (Ref. 6) tested these hypotheses experimentally and analytically on the Sn-Cd system, with the following results:

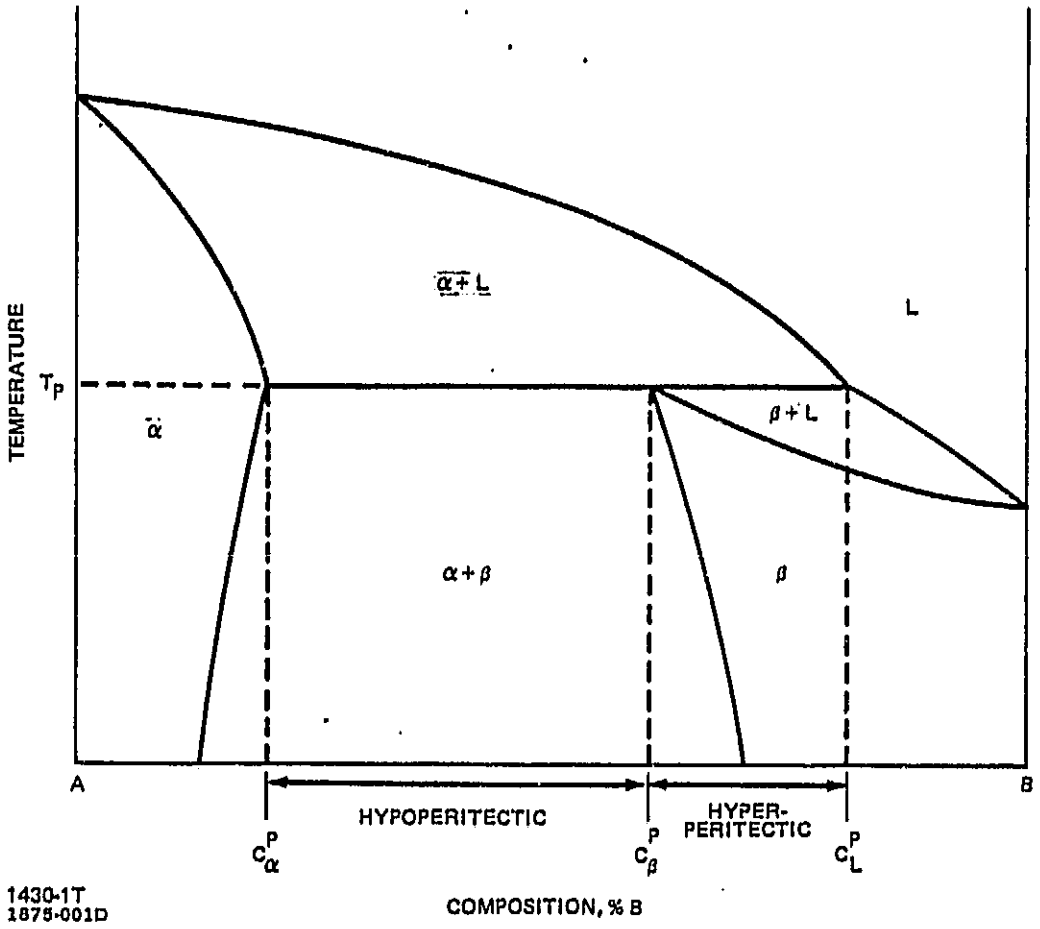

Fig. 1 Typical Peritectic Phase Diagram

- o Adaptation of the constitutional supercooling criteria to the peritectic case successfully predicted an approximate upper bound to the ratio of thermal gradient to solidification velocity (G/V) at which nonplanar (dendritic or cellular) growth occurs for hypoperitectic alloys
- o No coupled, eutectic-like, growth was observed
- o Those samples solidified at a G/V ratio in excess of that required by the constitutional supercooling criteria solidified with a planar interface but with a structure characterized by alternating bands of α and β arrayed perpendicular to the growth direction
- o Analysis similar to the Jackson and Hunt (Ref. 7) theory for lamellar eutectic growth was performed for a two-phase lamellar peritectic, and the undercooling versus velocity and lamellar spacing was found to be greatly different for the peritectic case.

It was concluded that the differences in the undercooling vs. velocity and lamellar spacing possibly precluded coupled growth in peritectic systems.

Titchener and Spittle (Ref. 8) reached similar conclusions from experiments they conducted on the Zn-Cu system. In addition, they noted macrosegregation in a thermally stabilized geometry for a (Zn-Cu) system presumed to exhibit density-driven thermosolutal convection, whereas they found no evidence of macrosegregation in a Sn-Sb nonconvecting system. Further, they suggested that the alternating planar band structure ceased when the bulk liquid composition, C_L, reached the liquidus composition, $C_L P$, of the peritectic isotherm, T_p.

An additional consideration, that of nonequilibrium peritectic solidification, was introduced by Kerr, Cisse, and Bolling (Ref. 9) and Scherbakov, David, and Brody (Ref. 10). The former suggested that, in addition to the equilibrium peritectic reaction, there is also the possibility of suppression of the peritectic transformation by solute supersaturation of the properitectic phase and concomitant undercooling. The latter suggest a non-equilibrium peritectic phase above the peritectic isotherm, i.e., β phase formation with superheating. These possibilities are superimposed on the equilibrium phase diagram in Fig. 2 for the Pb-Bi peritectic reaction under investigation. Both are shown to be energetically favorable in Fig. 3; that is, solidification occurs with a net reduction in free energy. Kerr, Cisse,

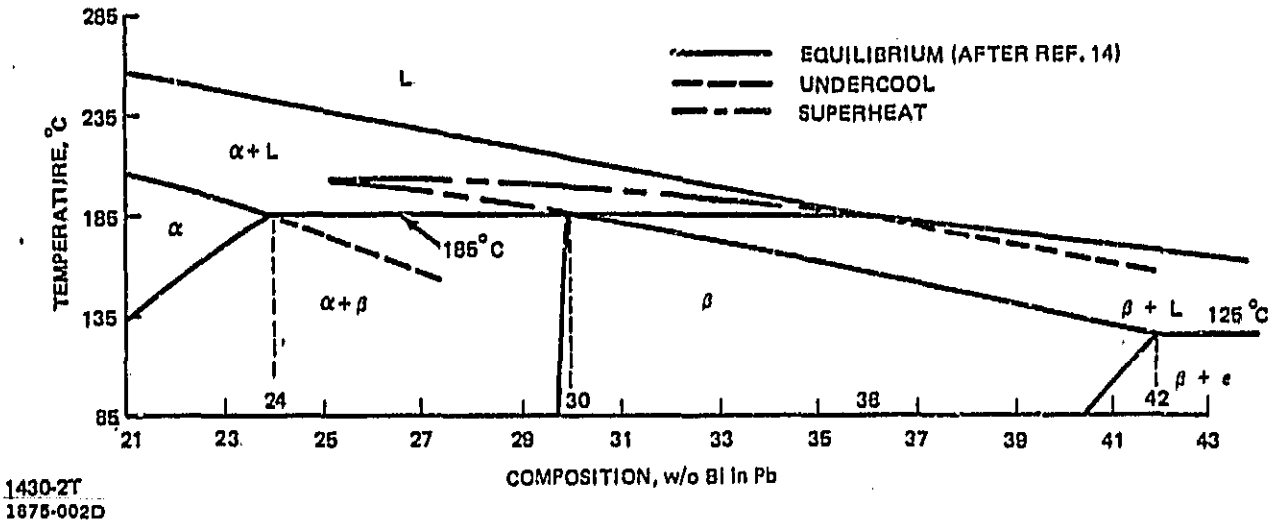

Fig. 2 Pb-Bi Peritectic Phase Diagram Segment with Proposed Metastable Solidification Reactions

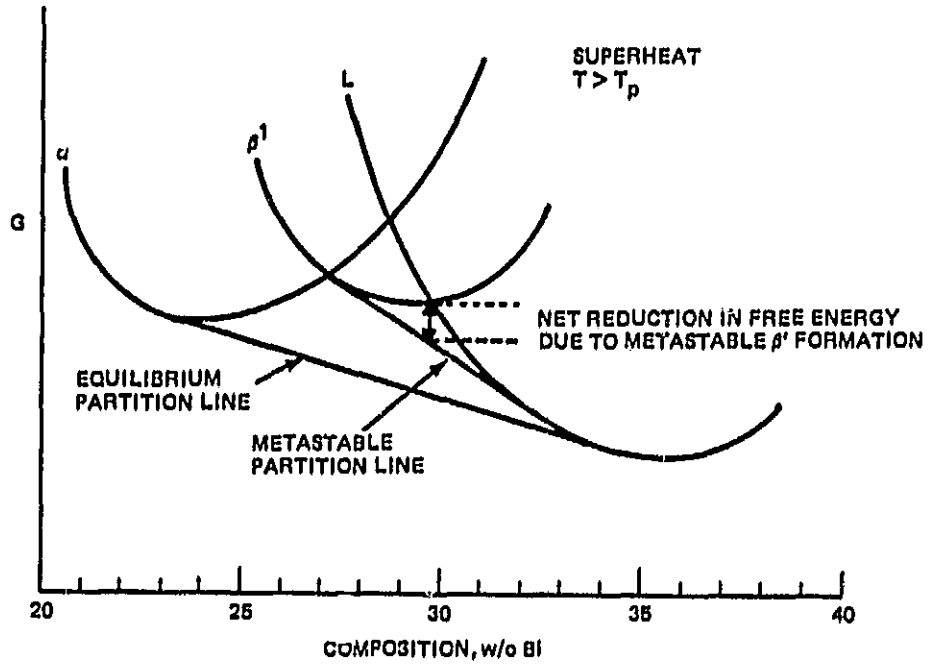

(a) Metastable Formation of β

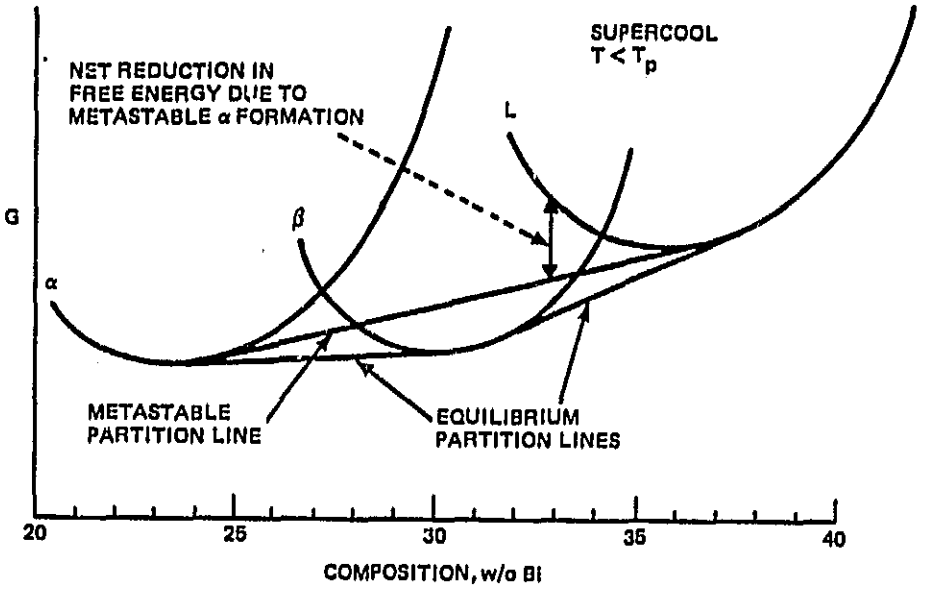

(b) Metastable Formation of α

1875-003D

Fig. 3 Schematic Free Energy Diagrams (a) Metastable Formation of β, (b) Metastable Formation of α

and Bolling (Ref. 9) offer support for the supercooling mechanism for high-rate dendritic solidification of Al-Ti alloys. Scherbakov, David and Brody (Ref. 10) support the superheat mechanism for plane-front solidification of hypoperitectic Pb-Bi alloys, although they made no measurement of local compositions.

Sundquist and Mondolfo (Ref. 11) indirectly support the supercooling mechanism in Pb-Bi alloys, reporting that the α phase will not nucleate the β phase above 167°C, in vacuum. However, Goddard and Childs (Ref. 12) report massive nucleation of β between 184 and 170°C in hyperperitectic alloys processed in air.

The present program was initiated to investigate solidification mechanisms encountered during plane-front directional solidification of peritectic alloys and to determine whether these mechanisms or the resulting morphologies are significantly influenced by gravitationally driven thermosolutal convection. The Bridgman-Stockbarger solidification technique was used.

The results of the first year's work on this project (Ref. 13) led to the conclusions that the Pb-Bi phase diagram of Predel and Schwermann (Ref. 14) is accurate over the compositional regime under investigation, 15-55 w/o Bi, and that constitutional supercooling criteria offer reasonable upper limits for dendritic solidification. Banding was noted, as was a region of refined $\alpha+\beta$ morphology which appeared to solidify isocompositionally. In addition, appreciable macrosegregation was noted during the directional solidification of all Pb-Bi alloys investigated and was attributed to thermosolutal convection. The macrosegregation pointed to the need for a peritectic solidification model that could account for partial mixing in the liquid ahead of the solidification interface. A candidate stagnant film peritectic solidification model was developed but was not tested experimentally. In the second-year's effort, we investigated:

- Origins of the thermosolutal convection noted in the Pb-Bi system;
- Mechanism of solidification within the compositional regime extending from the limit of terminal solid solubility and the peritectic composition;
- Convective influences on these solidification processes.

2. EXPERIMENTAL TECHNIQUES

2.1 ALLOY PREPARATION AND DIRECTIONAL SOLIDIFICATION

Starting Pb and Bi materials were 99.999% pure. Appropriate admixtures of Pb and Bi were weighed and encapsulated in 0.6 cm (outer diameter) synthetic quartz tubing, under a mechanical pump vacuum. These capsules were inductively heated and electromagnetically stirred for a 3 to 4 hr period at 600°C, and the molten alloy was then allowed to cool radially in the evacuated quartz ampoule. Alloys of principally 27 w/o Bi were prepared. These samples were readily removed from the ampoules, indicating minimal liquid/crucible interaction.

The samples were then machined to produce flat surfaces on the ends and an axial hole was drilled 2.38 cm deep, to accommodate an ultrafine thermocouple. The sample, in its entirety, was then incorporated into an instrumented growth ampoule. Final sample dimensions were typically 0.4 cm diameter and 6.5 cm length.

The ampoule design for directional solidification is shown in Fig. 4. The ampoules were instrumented with one Omega Engineering SCASS-010G-16 ultrafine chromel-alumel thermocouple probe. These probes consist of 0.0005 in. thermocouple wires packed with MgO insulation in a 0.010 in. stainless steel sheath.

Ampoules were processed in a Bridgman-Stockbarger directional solidification furnace. The furnace is shown schematically in Fig. 5. It is a resistance-heated Bridgman-Stockbarger furnace with active cooling in the chill block. Furnace translation velocity may be varied from 0.10 to 150 cm/h. The sample is held stationary on the centerline of the furnace. Temperature profiles over a range of power conditions are also shown in Fig. 5. Thermal gradients were typically varied from 50 to 150°C/cm and solidification velocities were varied from 0.05 to 1 cm/h in this study. Seed crystals were not used and melt-back interfaces were used only occasionally.

The temperature/time behavior during solidification was monitored using a Minc-II Data Acquisition System. The temperature vs time output was analyzed to determine the cooling rate in the solid and liquid and the solidification temperature. It was assumed that the solidification velocity was identical to

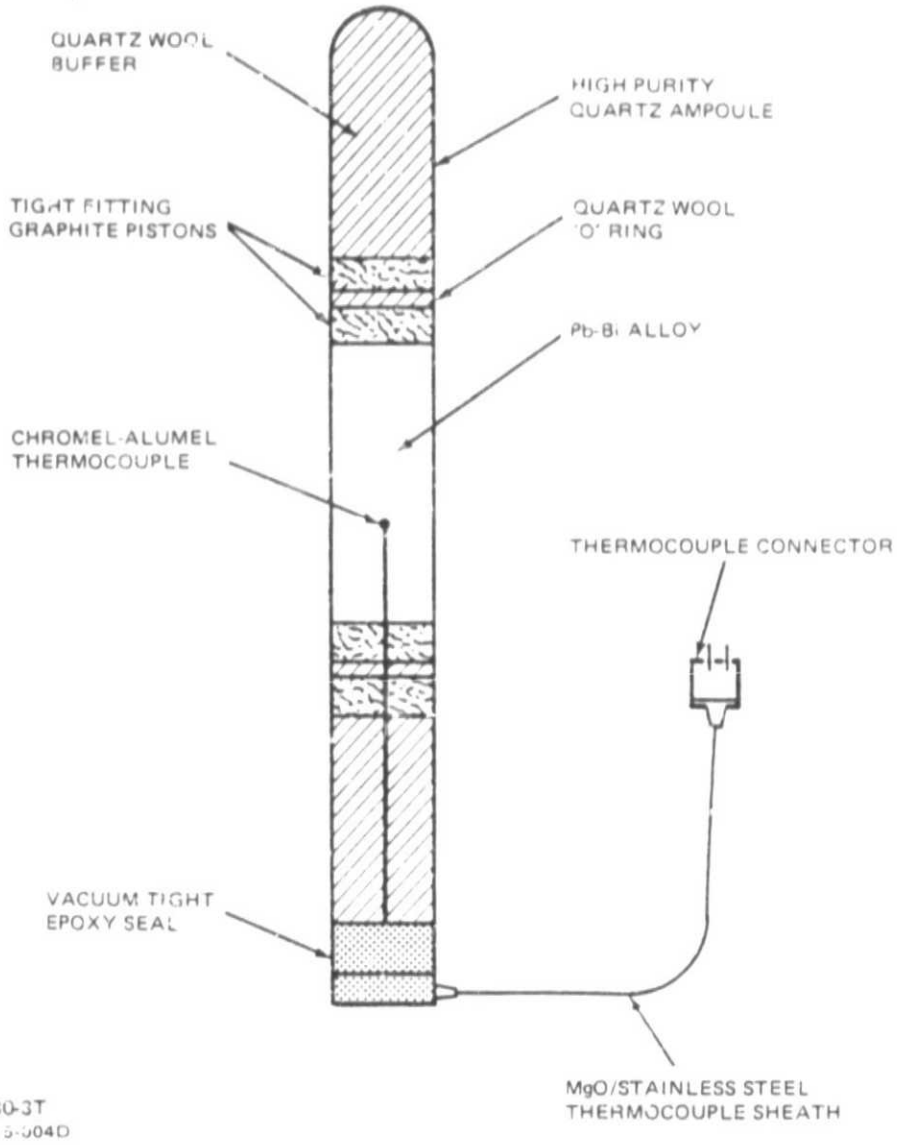

Fig 4 Ampoule Design For Pb-Bi Directional Solidification

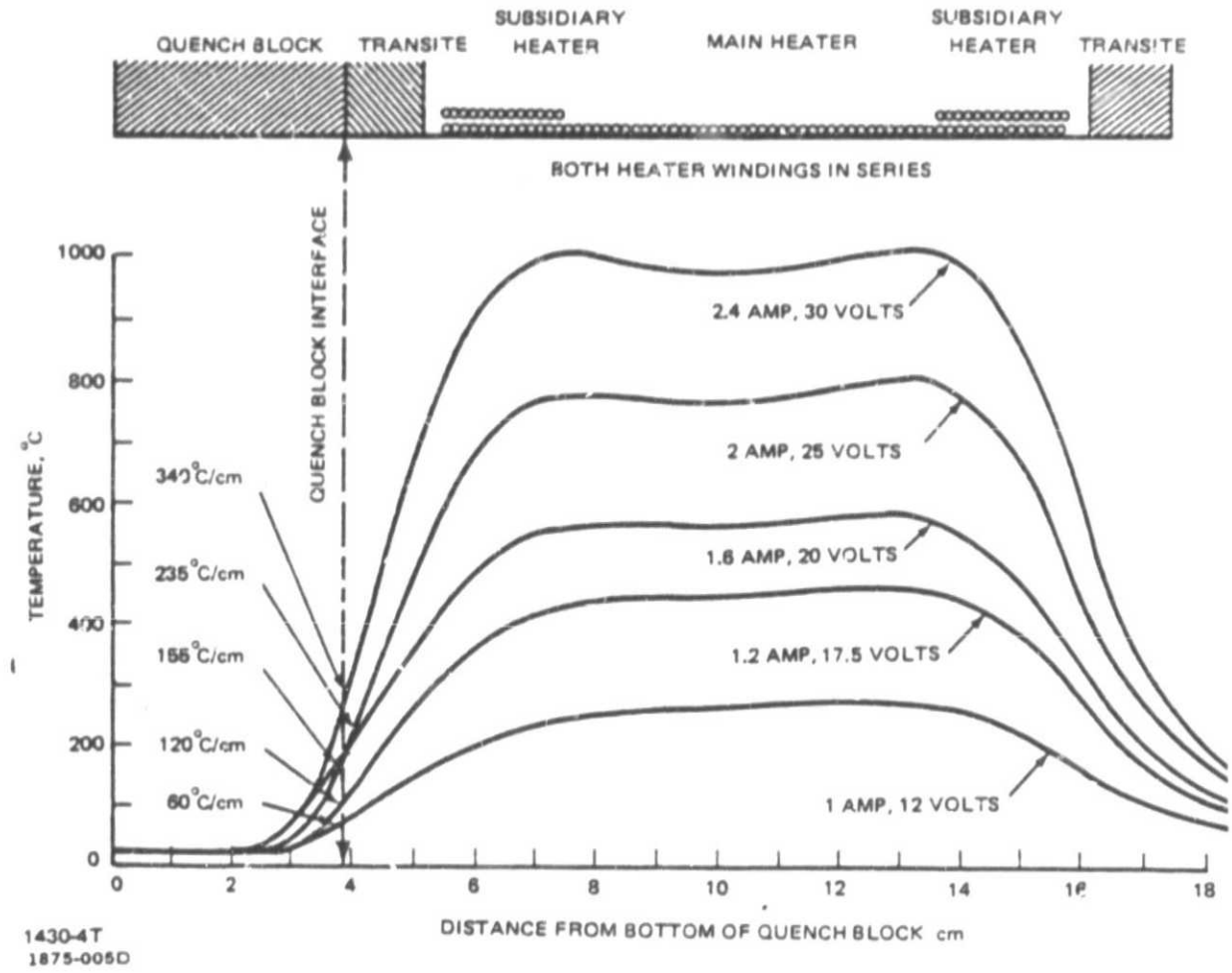

Fig. 5 Schematic Representation of Bridgman - Stockbarger Furnace & Characteristic Thermal Profiles

the furnace translation velocity, which was also monitored by the Minc-II. The thermal gradients in the solid and liquid were then calculated by dividing the cooling rate by the solidification velocity.

2.2. INTERFACE DEMARCATION

Since interface curvature is indicative of radial temperature gradients interface demarcation was a significant consideration in this work. Provision was made to allow the release of the growth ampoule from its stationary supports thus dropping the ampoule, for a vertical growth orientation, into an ice-water bath and quenching the solidification interface. This technique provided excellent results.

Interface demarcation was also attempted by periodically stopping the furnace translation for 30 min. It was hoped that the small difference in the location of the solidification isotherm between the cases with and without translation and the concurrent solute readjustment resulting from the rate changes in this region would provide demarcation of the solidification interface morphology. This was not as definitive as the interface quench technique and rate changes were abandoned. Figure 6a shows a typical quenched interface and 6b shows a rate-change interface.

Lastly, morphological transitions were encountered due to the aforementioned macrosegregation. These microstructural transitions were assumed to occur at specific compositions and temperatures, and would seem to offer direct insight into the configuration of the solidification isotherm. This could be complicated by radial compositional gradients, resulting from transverse flow at the solidification interface, and a non-isothermal temperature of solidification radially. This could result in significant curvature of the isocompositional morphological transition interface even though the isotherms in this region of the sample were planar.

2.3 X-RAY DIFFRACTION

Longitudinal and transverse metallographic sections of each Pb-Bi sample were analyzed using a Picker diffractometer. Copper Kα radiation at 36 kV and 30 mA was used throughout, with a nickel filter. The pulse height analyzer was used to maximize the peak to background ratio, and the angular regime from 5 to 135^{o} was investigated.

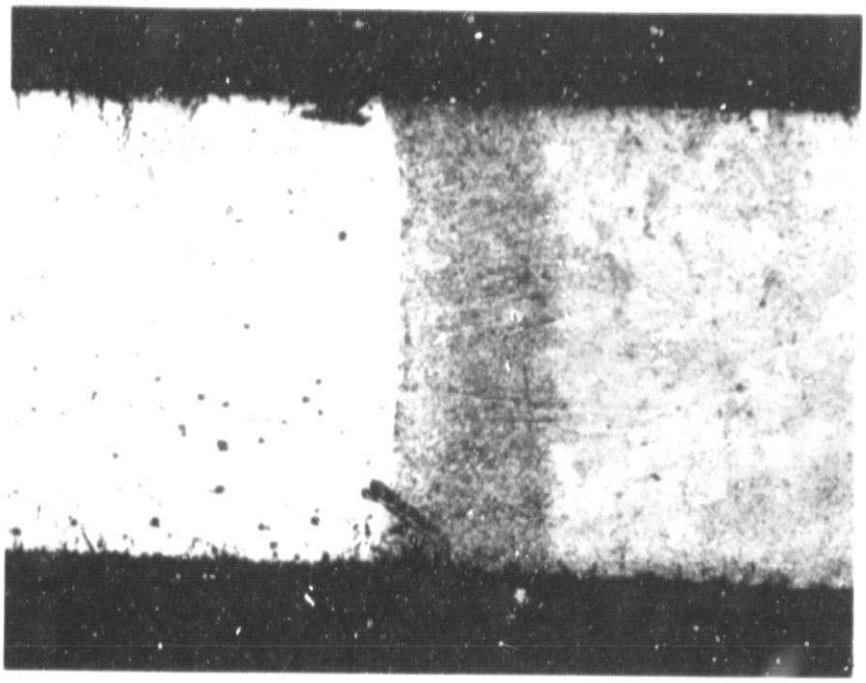

(a) Typical Quenched Interface. Properitectic α Crystals on Left, Quenched Liquid on Right

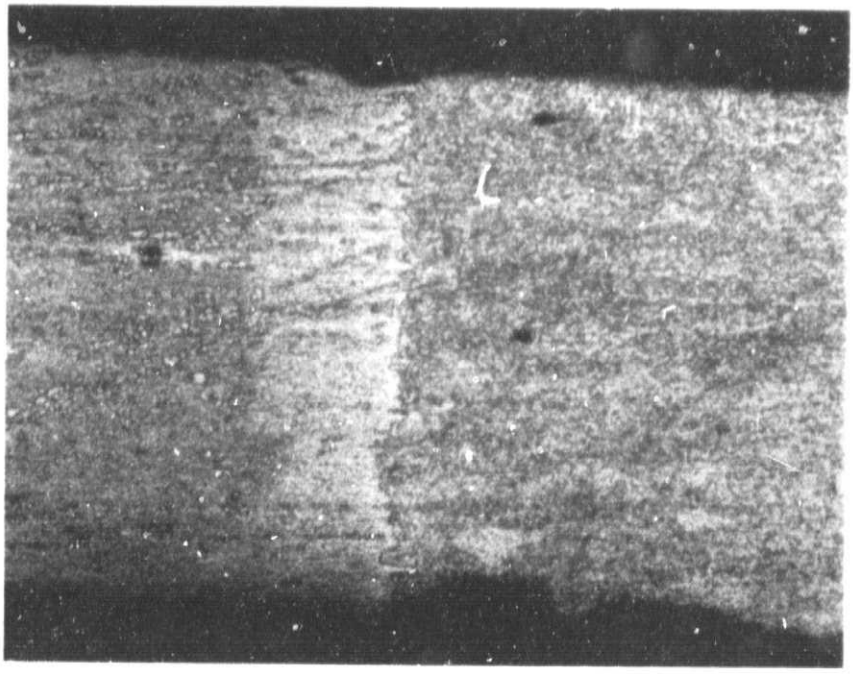

(b) Change Of Rate Interface

1875-006D

Fig. 6 Typical Hypoperitectic Interface Demarcation on Pb-28 w/o Bi Alloys, (a) Quenched Interface, (b) Change of Rate Interface

Experimental values of 2θ were corrected to true zero and converted to d spacings. The lattice parameters were then calculated using the Nelson-Riley method (Ref. 15). All peaks in each pattern were accounted for by equilibrium phases. The lattice parameter data of Cooper (Ref. 16) were used as reference values for the α-Pb (Bi) terminal solid solution and β- PbBi peritectic phase, at room temperature.

2.4 DIFFERENTIAL SCANNING CALORIMETRY (DSC)

DSC analyses were conducted in a Dupont 990 Thermal Analyzer in the heating and cycle modes. The temperature differential between the sample and an aluminum standard was monitored from 25 to 395°C. The analyzer was calibrated using pure Pb, In, and Bi.

Samples for DSC analysis were segments of directionally solidified Pb-Bi samples that had been chemically analyzed using a Norelco electron microprobe. These samples were first run in the heating mode, with a heating rate of 10°C/min. The sample was heated to above the liquidus temperature, where it was held for 5 min, and then was cooled at the programmed rate. The sample was then cycled a second time to compare the directionally solidified liquidus and solidus temperatures with results from a randomly nucleated sample. These results were interpreted with respect to the Pb-Bi phase diagram of Predel and Schwermann (Ref. 14), the microstructure of the region, the x-ray results, and the chemistry.

3 - RESULTS AND DISCUSSION

3.1 INTERFACE QUENCH STUDIES

Experimental results from the first year of effort on this contract (Ref. 13) showed that growth conditions sufficient to stabilize plane front directional solidification of the properitectic α and peritectic β phases of the Pb-Bi peritectic system resulted in substantial macrosegregation, even for thermally stabilizing growth orientations. For example, the chemical composition of a 28 w/o Bi alloy, directionally solidified at a G/V ratio of 5.3×10^6 ^{o}C s/cm^2, varied from 18 to 56 w/o Bi over the length of the sample This substantial level of macrosegregation was a vivid demonstration of the importance of mixing in the melt that resulted from convection, presumably gravitationally driven buoyancy convection.

Fitting the properitectic portion of the above example of macrosegregation with a stagnant film model resulted in a calculated fitting coefficient, $p\delta$, of approximately 0.1. This is indicative of a 90% overlap of the convective field over the diffusional field at the interface and results from a high degree of mixing in the melt. The origin of the vigorous mixing was not obvious since the samples were grown vertically upwards, a growth orientation that minimizes thermal convection in the melt. In addition, the Pb-Bi system is thought to have only a small driving force for solutal convection, and this should have been stabilized as well. It was hypothesized that radial temperature gradients were contributing to the convective flow. This hypothesis led to the interface demarcation studies.

Thermal modelling of the Bridgman-Stockbarger directional solidification process by Fu and Wilcox (Ref. 17) has shown that the curvature of a specific temperature (solidification) isotherm (for a given set of furnace temperatures, materials, and experiment conditions) is dependent on the final location of this isotherm within the adiabatic zone of the furnace. This is shown in Fig. 7. Briefly, increasing isotherm curvature will be experienced as the solidification isotherm moves toward either end of the insulation layer (adiabatic zone) of the furnace. Increased isotherm curvature obviously introduces increased radial thermal gradients which can drive convection even in the thermally stabilized orientation.

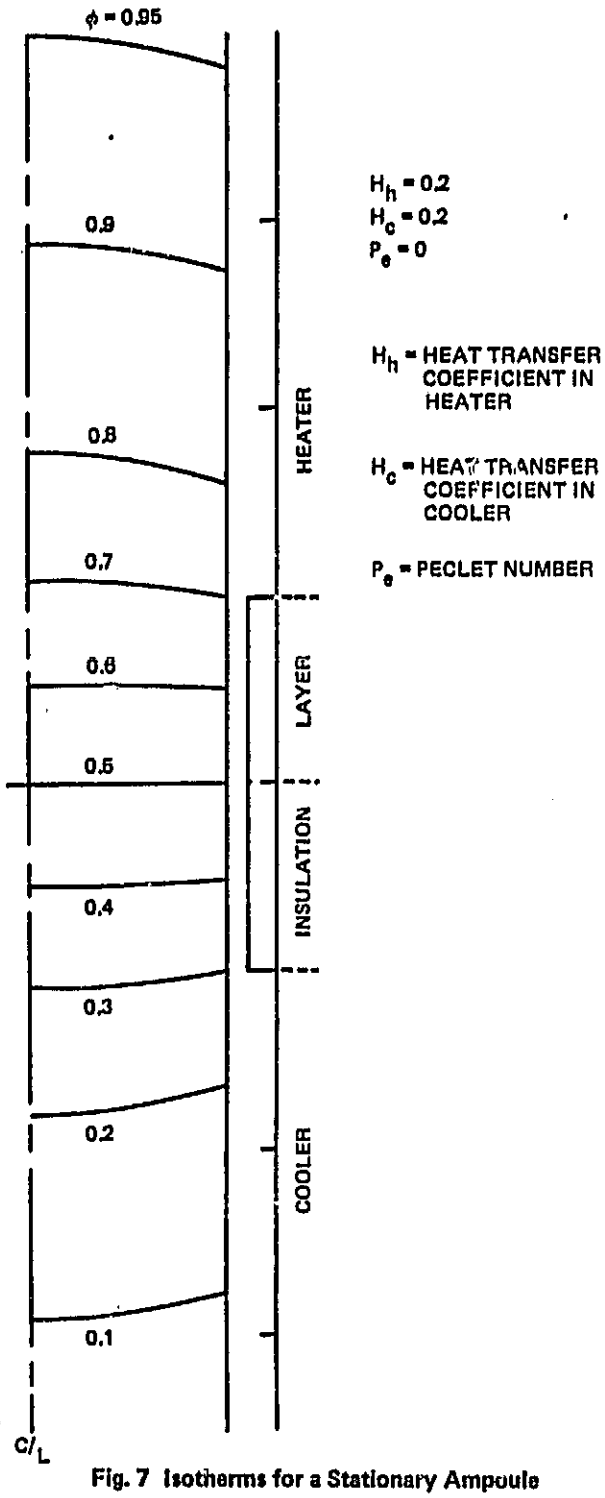

Fig. 7 Isotherms for a Stationary Ampoule

Carlson, et al (Ref. 18) have shown analytically, for the Bridgman-Stockbarger directional solidification geometry, that the flow configuration changes and the flow velocity increases when the solidification isotherm changes from planar to concave towards the liquid. Figure 7 shows that this occurs, for the heat transfer conditions cited, when the dimensionless temperature isotherm approaches 0.4. The dimensionless temperature, Φ, referred to above and in Fig. 7 is defined as:

$$\Phi = \frac{T_i - T_c}{T_h - T_c} \qquad (1)$$

where: T_i = isotherm temperature, T_h - heater temperature, and T_c = chill block temperature.

The isotherms of most interest in the Pb-Bi system are the solidification temperatures in the vicinity of the peritectic isotherm. For a 28 w/o Bi alloy, the equilibrium properitectic solidification is expected to range from 225 to 185°C. Equilibrium peritectic solidification would occur at 185°C and hyperperitectic solidification would occur between 185 and 125°C. Isotherms of particular significance to this effort, therefore, are 225, 185, and 125°C. Fig. 8 shows the variation of ϕ for the 225, 185, and 125°C temperatures as a function of furnace temperature, T_h. The chill block temperature, T_c, was assumed constant at 25°C for these calculations.

In our initial effort (Ref. 13), the furnace temperature, T_h, was 510°C, in order to maximize the longitudinal thermal gradient. The dimensionless temperatures for the 225, 185, and 125°C isotherms are 0.4, 0.34, and 0.21, respectively, for the 510°C furnace temperature. These are dimensionless temperature values that would lie near the cold end of the adiabatic zone and would be expected to be progressively more concave towards the liquid. The increasing concavity, and concomitant increasing radial thermal gradients, are an effective source of gravitationally driven convection.

As a result of these considerations, it was decided to conduct interface quench studies over a spectrum of furnace temperatures in order to select growth conditions for the Pb-Bi alloys that would minimize interface curvature.

Fig. 9 shows the properitectic interface shapes, for furnace temperatures of 360 and 410°C, determined by drop quenching the growth ampoule into ice

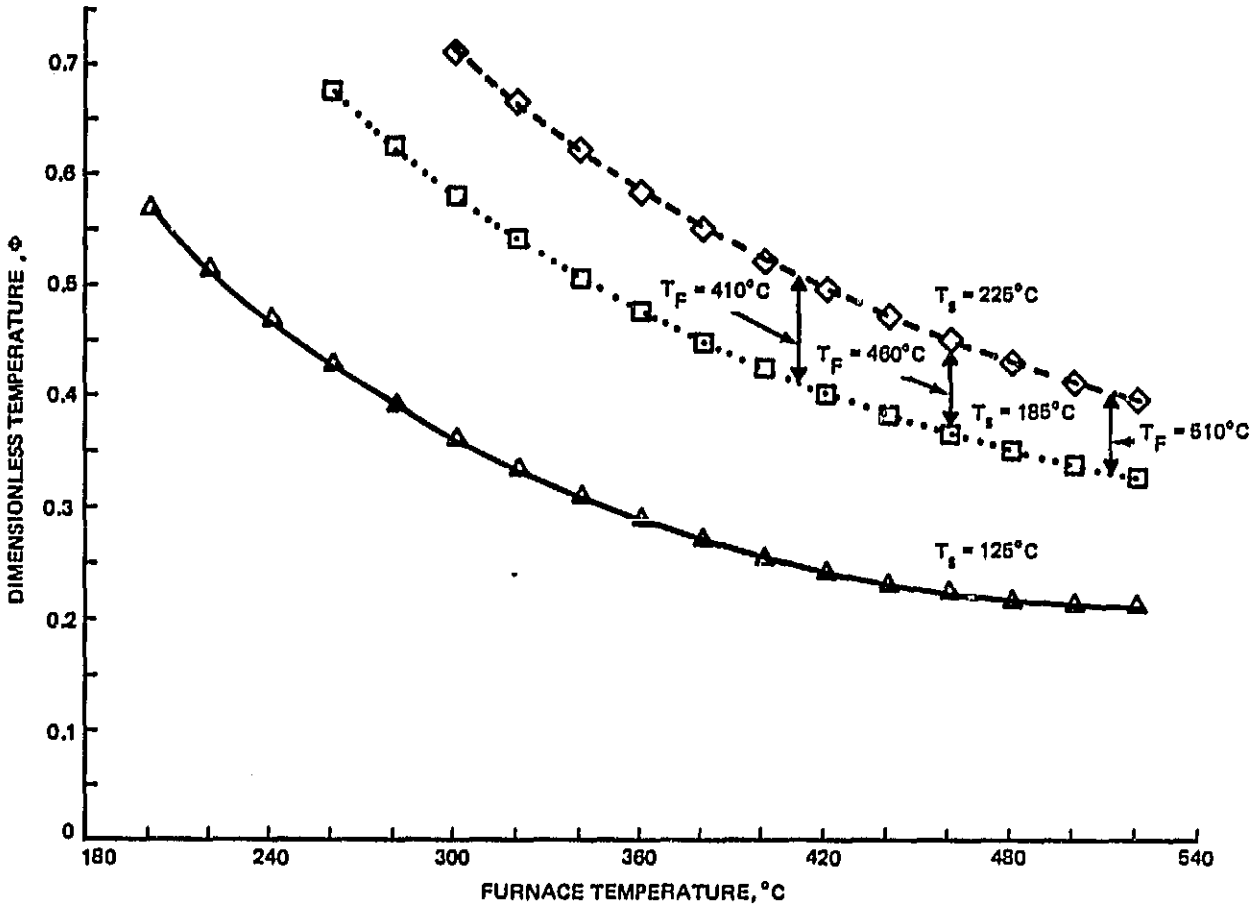

Fig. 8 Dimensionless Temperature, ϕ, as a Function of Furnace Temperature for the 225, 185, and 125°C Isotherms

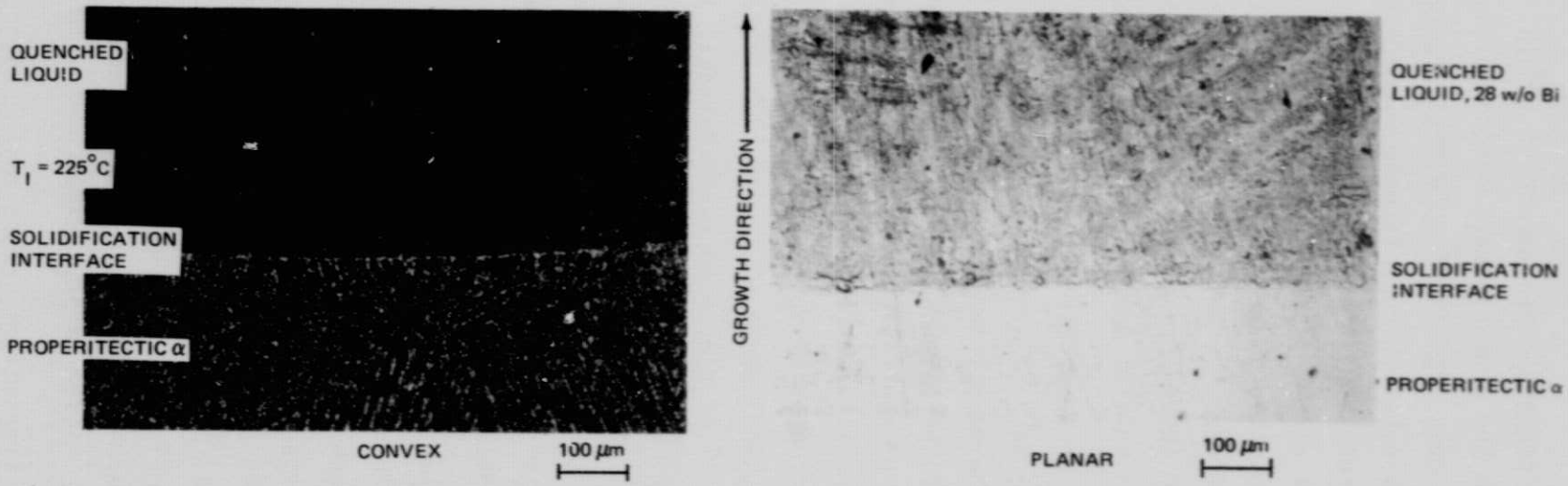

(a) T_f = 360°C, ϕ = 0.58

(b) T_f = 410°C, ϕ = 0.50

1875-009D

Fig. 9 Quenched Properitectic Interfaces Trend from Convex to Planar as Furnace Temperatures are Increased & Dimensionless Temperatures, ϕ, of Solidification Interface are Decreased (a) 360°C, ϕ = 0.58 and (b) 410°C, ϕ = 0.50

water, after growing a predetermined amount of sample. The interfaces quenched were from both the properitectic or peritectic regions of growth, that is, the region of most significance to this study. It is clear that the interface quenched from a test with a furnace temperature of 360°C is convex towards the liquid whereas the interface quenched from a test with a furnace temperature of 410°C is almost planar (very slightly convex). A furnace temperature of 510°C resulted in an interface concave toward the liquid. Furnace temperatures of 410°C were used throughout this study. During the latter stages of growth (hyperperitectic solidification) some highly complex interface shapes due to solutal flows were encountered, as shown in Fig. 10.

Lowering the furnace temperature also lowered the longitudinal thermal gradient imposed on the solidification interface. As a consequence, if the same G/V ratio was to be maintained for the purpose of interface stability, then the velocity had to be proportionally reduced. If all other factors remained constant, the $p\delta$ coefficient would be expected to be proportionally reduced since it is directly proportional to velocity. Since the velocity was typically reduced by a factor of 2, the $p\delta$ value anticipated by these process changes would be ~0.05, indicative of a very high degree of mixing. In fact, for the samples that will be discussed quantitatively in Section 3.4, the experimental value of $p\delta$ was approximately 0.30 ± 0.05 which is indictive of a greatly reduced level of convection. Thus it was concluded that much of the convection experienced by the samples processed at 510°C resulted from the radial thermal gradients driving gravitationally driven convection.

3.2 MORPHOLOGICAL TRANSITIONS

The macrosegregation that occurs during the plane front directional solidification of the Pb-Bi alloys, imposes significant compositional variation over the length of the sample as a function of the fraction solidified. As a consequence, as the composition changes from one region of the phase diagram to the next, there are discrete phase boundaries identifying the transition from one set of phase relations to the next. The growth morphology within each of these regions differs according to morphological stability criteria, thermal geometry, solute redistribution, and the crystallographic growth habits of the phases.

The morphological transitions, based on the equilibrium phase diagram, are such that solid compositions in excess of 24 w/o Bi would be expected to

Fig. 10 Morphological Transition Showing Highly Complex Interface Morphology, with a Reentrant Corner, Resulting from Thermo-solutal Flows Across the Solidification Interface

be two phase arrays of $\alpha+\beta$, up to compositions of 30 w/o Bi. Single phase β would be expected to form between 30 and 42 w/o Bi. In both cases, solid state precipitation of a second phase may be exected on cooling due to a receding solvus line. PbBi, β, is expected to precipitate from terminal solid solution α and ϵ is expected to precipitate from saturated β.

The morphological transition from properitectic α to $\alpha + \beta$ solidification can occur as a planar/planar or planar/nonplanar transition depending on test conditions and morphological stability. At low values of G/V the $\alpha + \beta$ region will be dendritic (nonplanar, non-isothermal) whereas at high values of G/V the $\alpha + \beta$ region appears monolithic (planar). A planar to nonplanar transition, from α to $\alpha + \beta$ is shown in Fig. 11a. The planar to planar α to $\alpha+\beta$ transition, however, is not morphologically distinct, appearing to be continuous with the properitectic α solidification and so will not be illustrated. The planar $\alpha + \beta$ region had a slightly different luster (buff instead of silver) after mechanical polishing and rinsing and was frequently heavily twinned. The origin of the twins is uncertain and could be due either to the mechanical polishing technique or to a massive transformation.

The properitectic α region of the plane front solidified samples is characterized by large grains of terminal solid solution α with an extremely fine dispersion of β which has precipitated from the supersaturated solid solution on cooling below the $\alpha/\alpha+\beta$ solvus temperature, as shown in Figure 11b. These particles were extremely difficult to photograph because of their very small size and the absence of contrast in both the optical and scanning electron microscopes. The β precipitates appear to be small spheroids in a homogenous array.

The region of the sample which is compositionally in the $\alpha+\beta$ two-phase region of the equilibrium phase diagram consists of a very fine mixture of α and β, similar in appearance to the properitectic α region. This region had a different luster than the properitectic α region and was usually heavily twinned as previously noted. The twinned microstructure is shown in Fig. 12a. The twinned region changes on aging at room temperature over a period of months and develops into a coarse cellular structure, as shown in Fig. 12b.

Initially it was assumed that the cellular structure was due to a lamellar eutectoid decomposition which occurs at cryogenic temperatures (-64^{0}C, Ref.14), since the samples had been stored in liquid nitrogen after

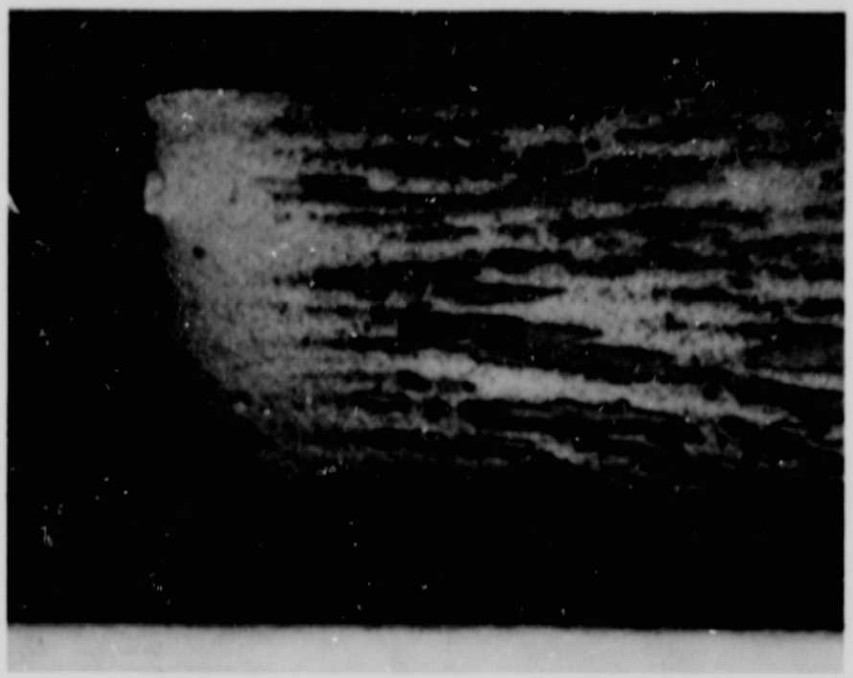

(a) Planer to Non-Planer ($\alpha \rightarrow \alpha + \beta$) Morphological Transition in Pb-28 w/o Bi Alloy

(b) β Precipitation in α Matrix

1875-011D

Fig. 11 Alpha (α) and Alpha + Beta ($\alpha + \beta$) Morphologies (a) Planar to Non-Planar Solidification Structure (b) Beta (β) Precipitation in Alpha (α) Matrix

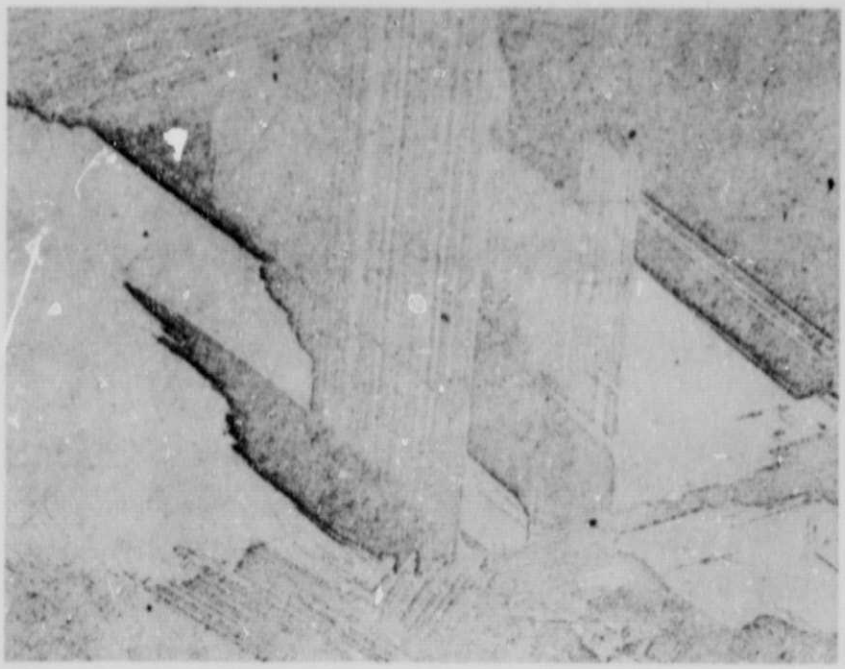

(a) Twinned Region As Grown in Pb-28 w/o Bi Alloy Solidified Under Plane Front Conditions

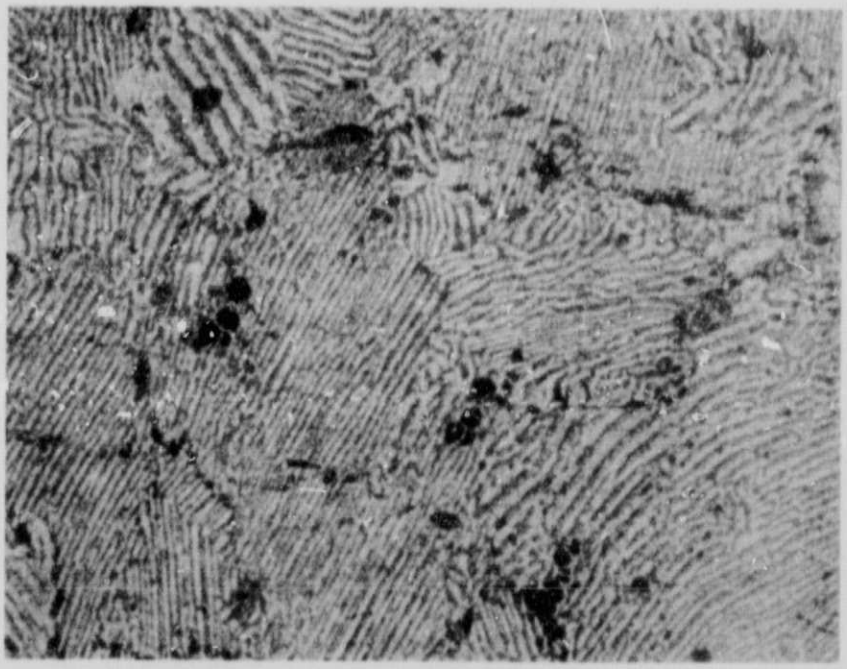

(b) Twinned Region Above Aged At Room Temperature For Several Months Showing Cellular Precipitation

1875-012D

Fig. 12 Microstructures of Regions Compositionally Within the Two Phase ($\alpha + \beta$) Phase Field, (a) As Grown, (b) Aged at R.T.

growth and prior to analysis. This was disproved however when subsequent samples, stored only at room temperature, showed a similar microstructural development. This structure will be discussed in detail in subsequent quantitative x-ray results and conclusions sections.

The $\alpha + \beta$ to β transition can occur as a nonplanar transition as well as a planar to planar transition. Figure 13a shows the nonplanar/planar transition from $\alpha + \beta$ to β and Fig. 13b shows the planar/planar transition that our work (Ref. 13) described last year. The planar/planar transition shown in Fig. 13b is characterized by alternating bands of $\alpha+\beta$ and β arrayed perpendicularly to the solidification direction. This morphology, termed 'banding', is reported to be the expected microstructure for the plane front solidification of the two-phase $\alpha+\beta$ compositional field rather than the desired coupled eutectic-like growth (Ref. 6,9). Banding has been reported in both convectively stabilized (Ref 6,9) and destabilized (Ref. 9) alloy systems. As a consequence, banding was thought to be characteristic of plane front peritectic solidification.

Surprisingly, flattening the solidification interface, with concomitant reduction in the level of convection experienced by the interface, eliminated the banded morphology, as shown in Fig. 13c. We have concluded that the oscillatory morphology, banding, is the result of thermal and/or compositional instabilities resulting from convection and is not a morphology inherent to peritectic plane front solidification. Therefore, the possibility of coupled peritectic solidification was pursued further.

The region of these convectively 'stabilized' samples which preceded the planar morphological transition to β was compositionally in the two-phase $\alpha+\beta$ region of the equilibrium phase diagram, typically 27 to 28 w/o Bi. The as-solidified structure of this region consisted of a very fine dispersion of β in a matrix of α. The crystallographic orientation of phases was consistent with the properitectic portion of the sample.

The plane front growth of β resulted in single or bicrystals of β growing with the <0001> direction parallel to the solidification direction. As the composition of β phase became progressively more enriched in bismuth, however, solid state precipitation of ε was encountered. The precipitation that occurred at the lowest temperatures appeared as a network of ε, reminiscent of a subgrain boundary precipitate, as shown in Fig. 14a. As the temperature of

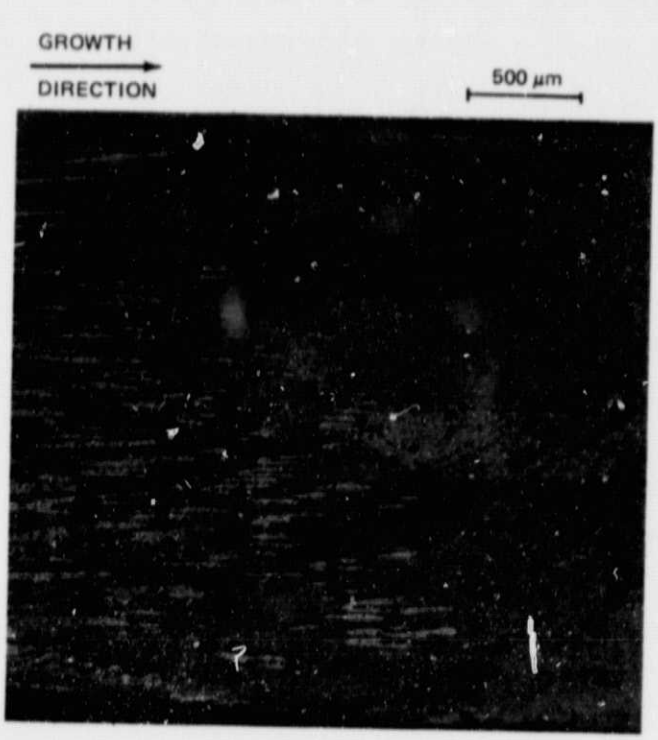

(a) Non-Planar to Planar ($\alpha + \beta \rightarrow \beta$) Morphological Transition in Pb-28 w/o Bi Alloy

(b) Banded Planar Transition Between $\alpha + \beta$ and β in Pb-27 w/o Bi Alloy

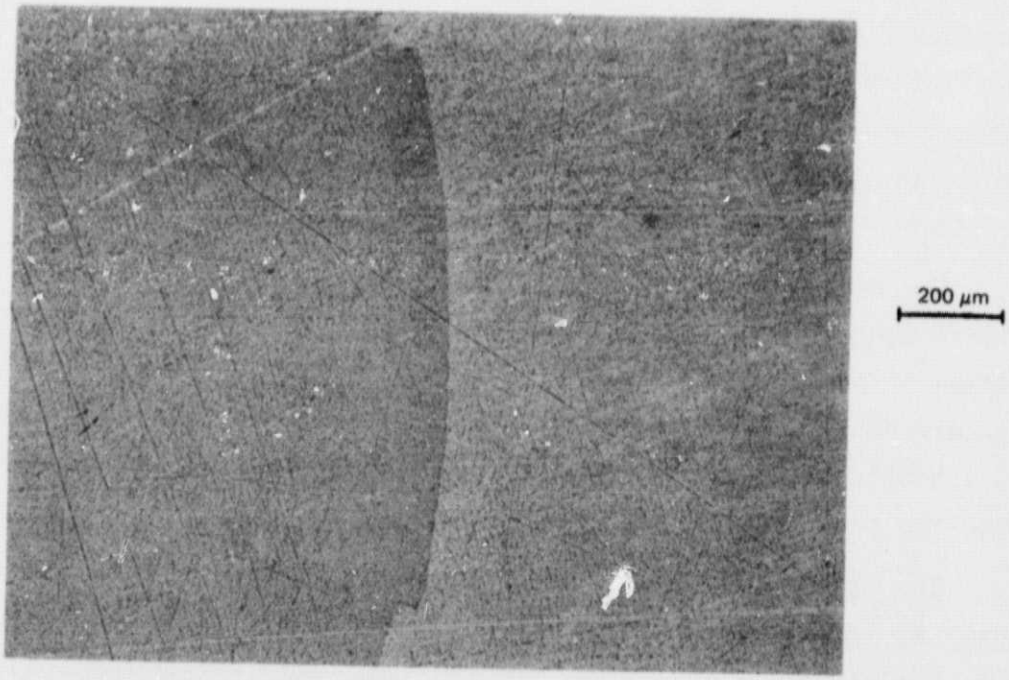

(c) Planar to Planar $\alpha + \beta$ to β Transition in a Pb-28 w/o Bi Alloy Solidified Under Stabilized Plane Front Conditions

1875-013D

Fig. 13 Two-Phase $\alpha + \beta$ to β Morphological Transitions (a) Non-Planar to Planar, (b) Banded Planar to Planar, and (c) Planar to Planar

(c) Aligned Epsilon, ϵ, Solid State Precipitation from PbBi, β, Precipitated During Directional Solidification

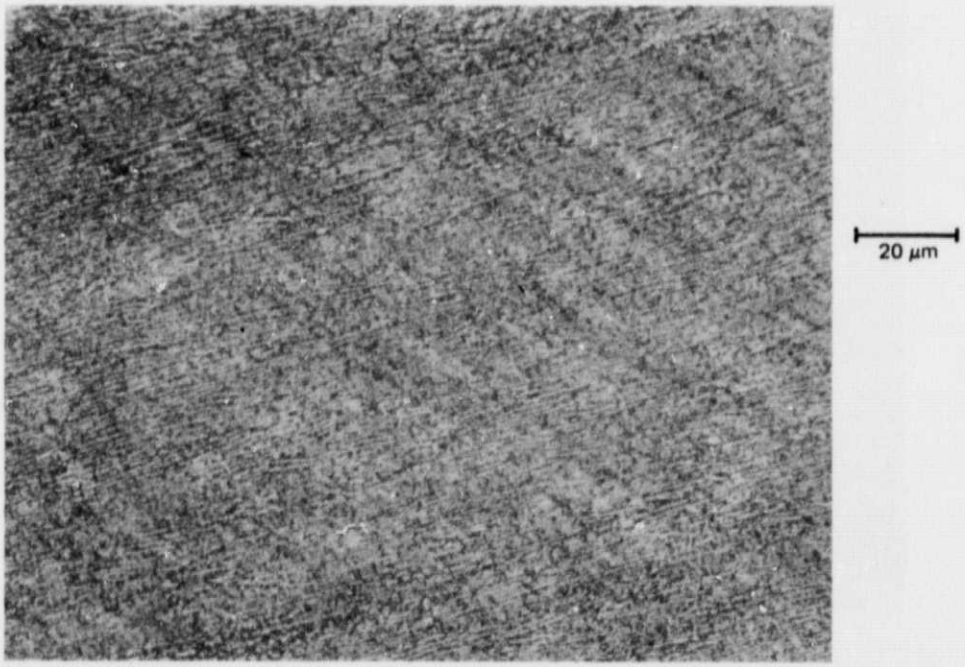

(d) Aligned Epsilon, ϵ, Solid State Precipitation from PbBi, β, Precipitated During Directional Solidification

1875-015B

Fig. 14 Epsilon, ϵ, Solid State Precipitation From Parent PbBi, β, Peritectic Phase (Sheet 2 of 2)

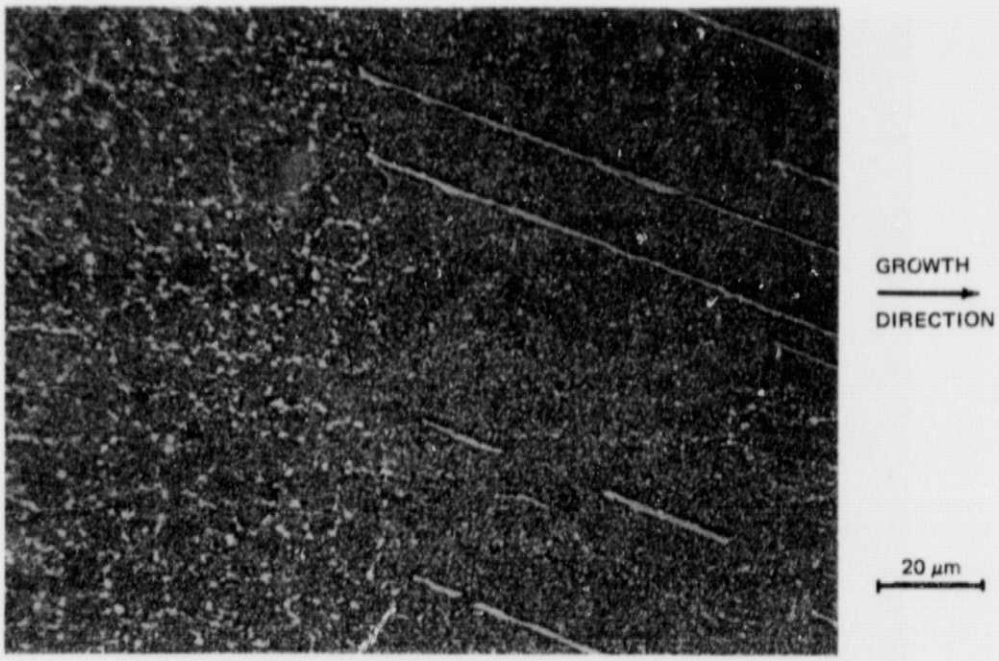

(a) Non-Aligned Epsilon, ϵ, Solid State Precipitation from PbBi, β Precipitation is a Network on the Left and Lath-Like on the Right

(b) Epsilon, ϵ, Precipitation from PbBi, β

1875-014D

Fig. 14 Non-Aligned, Lath-Like, Epsilon, ϵ, Solid State Precipitation from the Parent PbBi, β Peritectic Phase (Sheet 1 of 2)

precipitation increased the thermal gradient coincident with the precipitation also increased and the precipitate morphology changed to one of parallel arrays of laths of ε arrayed at an angle to the solidification direction. This is also shown in Fig. 14a and in 14b. The lath diameter and inter-lath spacing diminished with increasing precipitation temperature and local gradient at constant velocity, as shown in Fig. 14c and 14d, until the off-eutectic Liquid to β + ε solidification reaction was encountered. This reaction could not be morphologically stabilized and in all cases the solidification morphology consisted of proeutectic grains or dendrites of β surrounded by the irregular β+ε eutectic, as shown in Fig. 15a. The terminal region of some samples extended all the way to the β+ε eutectic composition and the microstructure in this region is shown in Fig. 15b.

3.3 DIFFERENTIAL SCANNING CALORIMETRY (DSC)

Morphologically interesting sections of directionally solidified samples were characterized using DSC to determine whether there was any evidence for metastable phase formation. It was anticipated that such evidence would be manifested as deviations from the equilibrium phase relationships of Predel and Schwerman (Ref. 14).

Morphologically distinct regions of three directionally solidified samples were investigated. These samples and their morphologies are illustrated in Fig. 16. Basically, four characteristic regions were investigated with two permutations added. These regions included: the properitectic α region, the isocompositional two-phase α+β region in the twinned and lamellar states, hyperperitectic β and the off-eutectic β+ε both as directionally solidified and as quenched liquid.

The results for the properitectic α region are shown in Fig. 17. For the unsaturated properitecitc α, which precluded solid state β precipitation, < 15 w/o Bi, there is no evidence of peritectic melting and the DSC trace is a single major peak. This was typical of the α region in sample Q-14. For regions slightly richer in bismuth, the peak associated with the peritectic isotherm appeared. This is shown in Fig. 18.

As the solidification progresses into the α+β equilibrium compositional regime, the DSC traces remain the same qualitatively, but differ quantitatively in that the magnitude of the peritectic peak increases. The magnitude

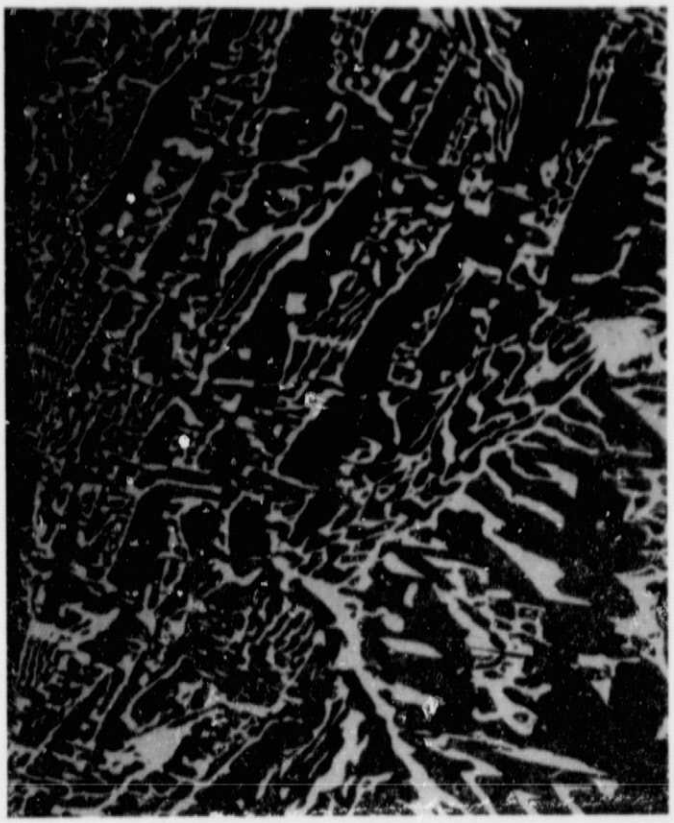

(a) Morphological Transition From Hyperperitectic β to Off-Eutectic $\beta + \epsilon$

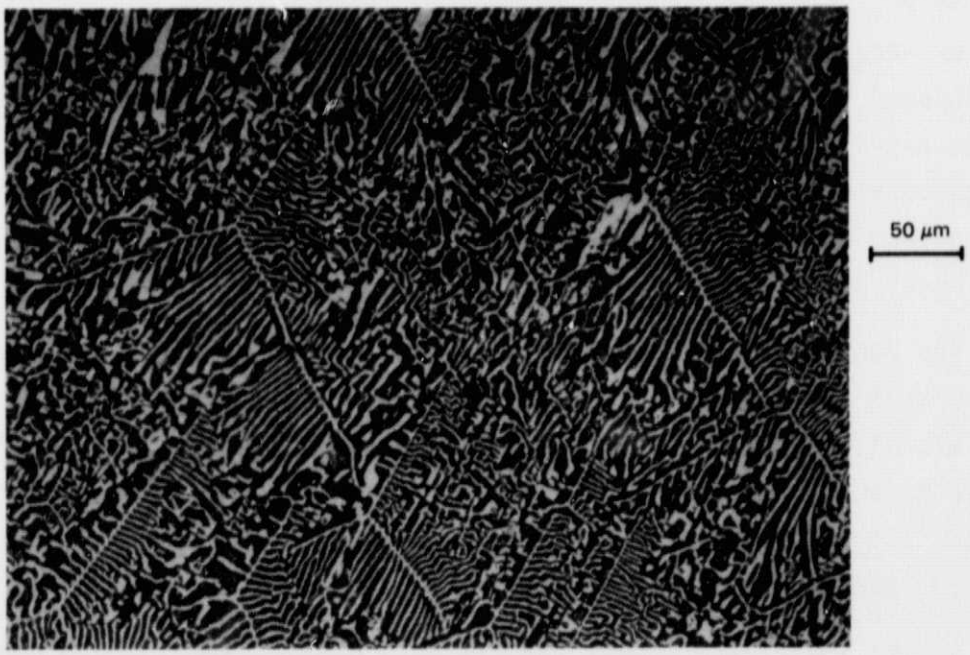

(b) Eutectic $\beta + \epsilon$ Microstructure

1875-015A

Fig. 15 Off-Eutectic (a) and Eutectic (b) $\beta + \epsilon$ Pb - Bi Microstructures

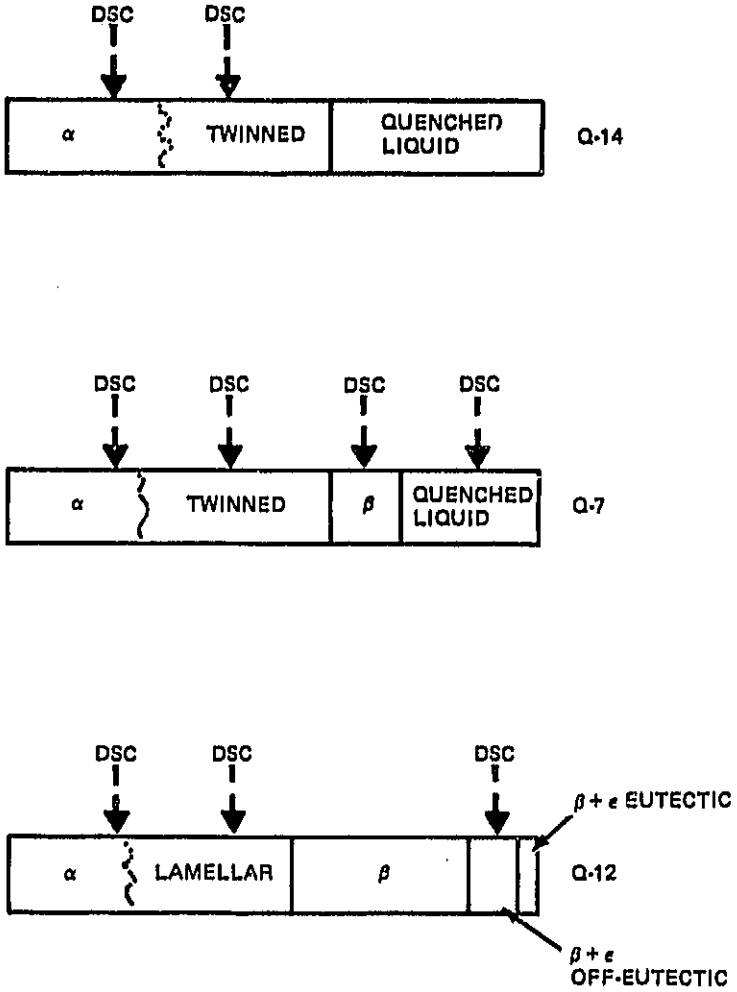

Fig. 16 Schematic Representations of Sample Regions Investigated Using DSC. Bulk Sample Compositions were Pb-28 w/o Bi

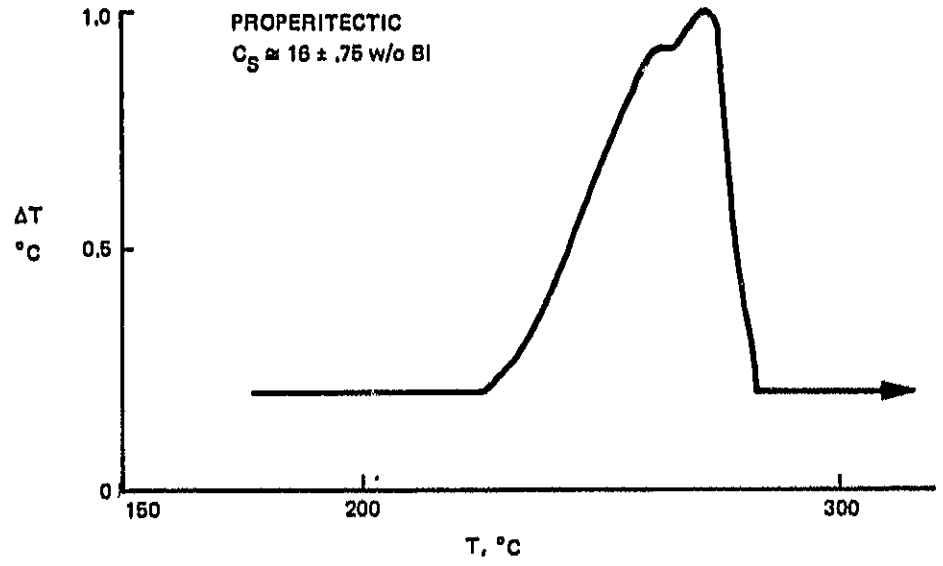

1875-017D

Fig. 17 DSC Melting Trace for Unsaturated Properitectic Terminal Solid Solution α - Pb, Showing No Evidence of Peritectic Melting

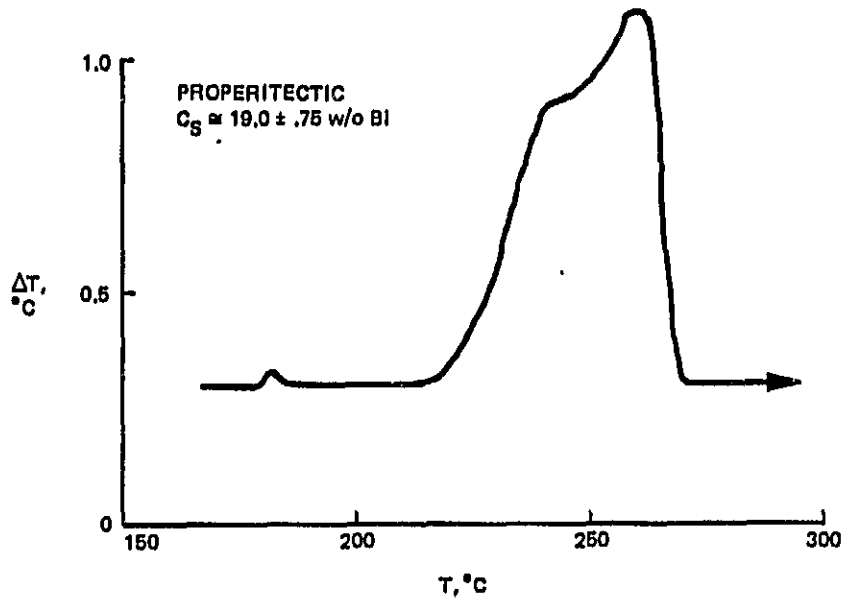

1875-018D

Fig. 18 DSC Melting Trace Typical of Saturated Properitectic α and Hypoperitectic Samples with Small Amount of Peritectic β

of the peritectic peak increases significantly as the room temperature aging takes place. This may infer that the as-grown, twinned, structure consists of a supersaturated properitectic α and that this supersaturated α ages at room temperature, forming the cellular structure and approaching equilibrium phase distribution, which is higher in β content.

Fig. 19 also shows the DSC traces for the hyperperitectic β and off-eutectic quenched liquid and directional solidification cases. These cases are unambiguous and simply illustrate that the samples conform to the equilibrium phase relations in this compositional regime.

In summary, no evidence was found for metastable phase formation, the DSC results being entirely explicable on the basis of equilibrium phase relations. The DSC traces proved to be reasonably consistent with the equilibrium behavior anticipated from the predetermined chemistries, and any deviations form equilibrium phase relations could be explained on the basis of convective influence on redistribution coefficients and macrosegregation.

3.4 CRYSTALLOGRAPHY

The crystallography of the terminal solid solution Pb phase, α, is face centered cubic (FCC) with the lattice parameter, a_o, increasing with increasing Bi concentration, as shown in Fig. 20. The data shown as diamonds are from Ref. 20 whereas those shown as circles are from the work of Cooper et al (Ref. 16). The latter will be used as reference values throughout the balance of this work for both the α and the β phases. The usual solidification growth system for Pb is the [100] direction on (110) planes.

The crystal structure of the Pb-Bi intermetallic phase, β,is hexagonal close packed (HCP) with the lattice parameters a and c increasing with increasing Bi content, as shown in Figs. 21a and 21b, after Cooper (Ref. 16). The usual relationship between the FCC and HCP phases is shown in Fig. 22 (Ref. 19) and, relative to the FCC phase, the HCP phase is expanded in the c direction and contracted in the a directions. The (0002) HCP plane is parallel to the (111) FCC plane, the $[10\bar{1}0]$ HCP direction is parallel to the $[1\bar{1}0]$ FCC direction, and the [0001] HCP direction is parallel to the $[\bar{1}1\bar{1}]$ FCC direction. Directional solidification for HCP crystals is usually in the [0001] direction, frequently but not always, on the $(10\bar{1}0)$ prismatic planes.

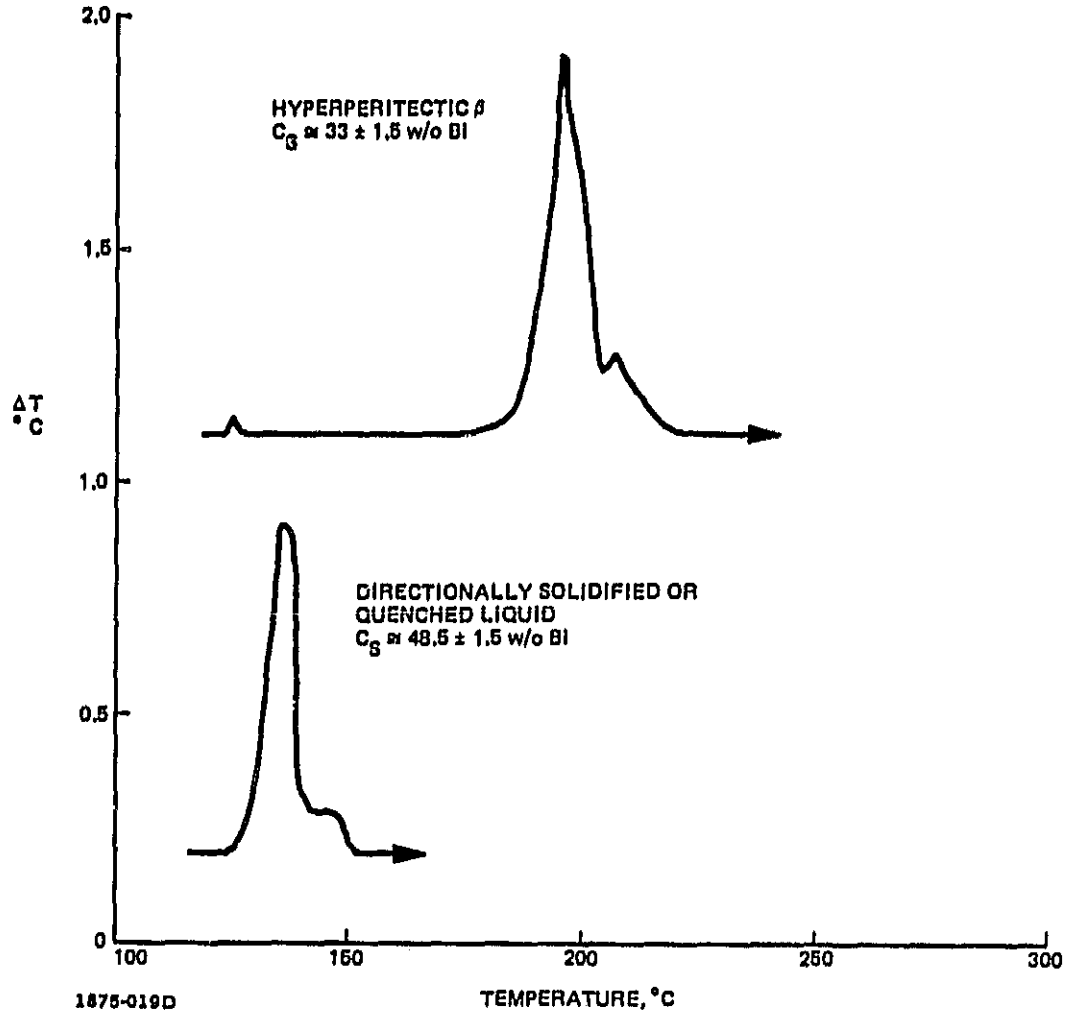

Fig. 19 DSC Traces For Slightly Hyperperitectic β And Off-Eutectic β + ε Sample Segements

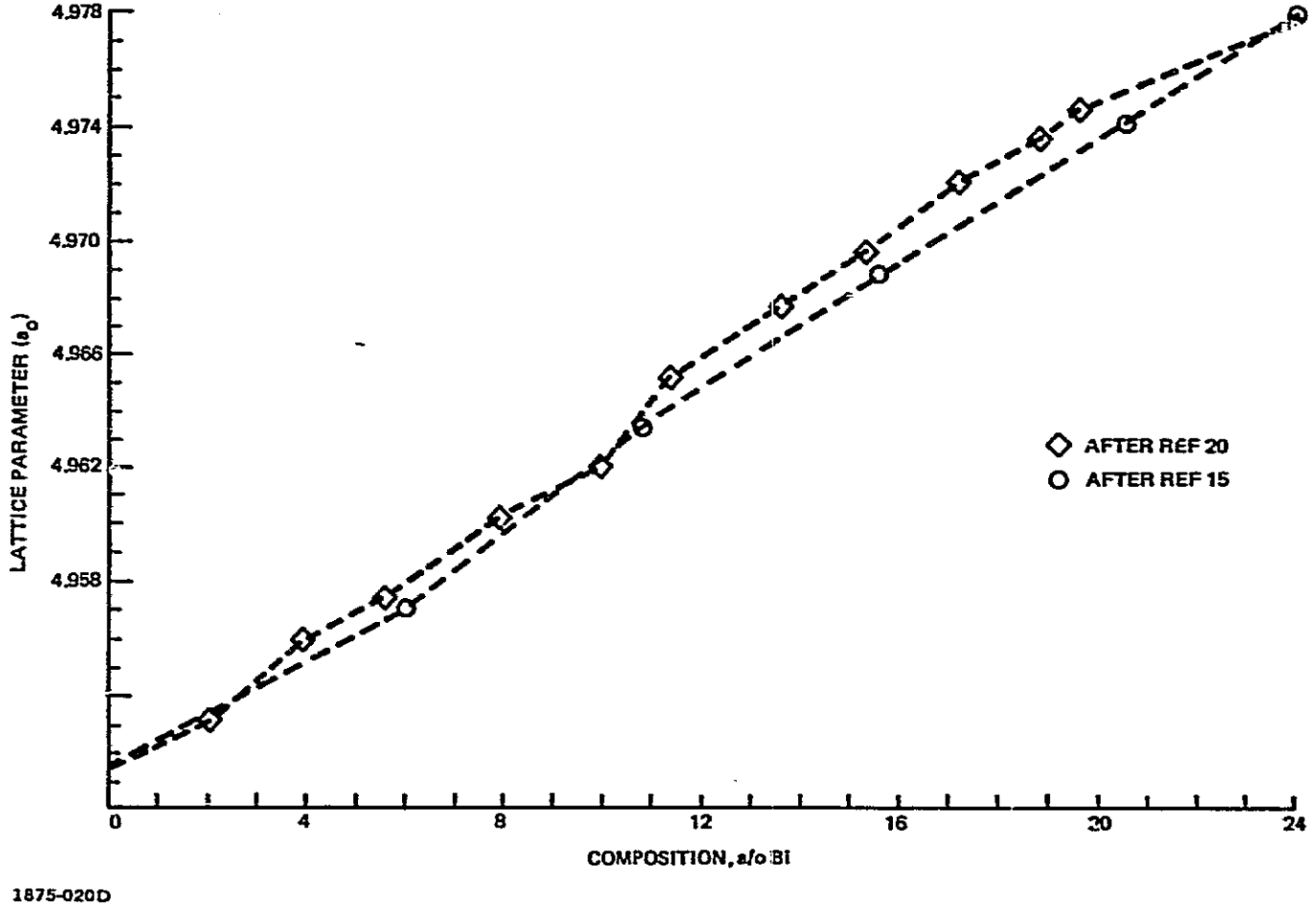

Fig. 20 Lattice Parameter, a_o, of Terminal Solid Solution Pb as a Function of Bi Concentration

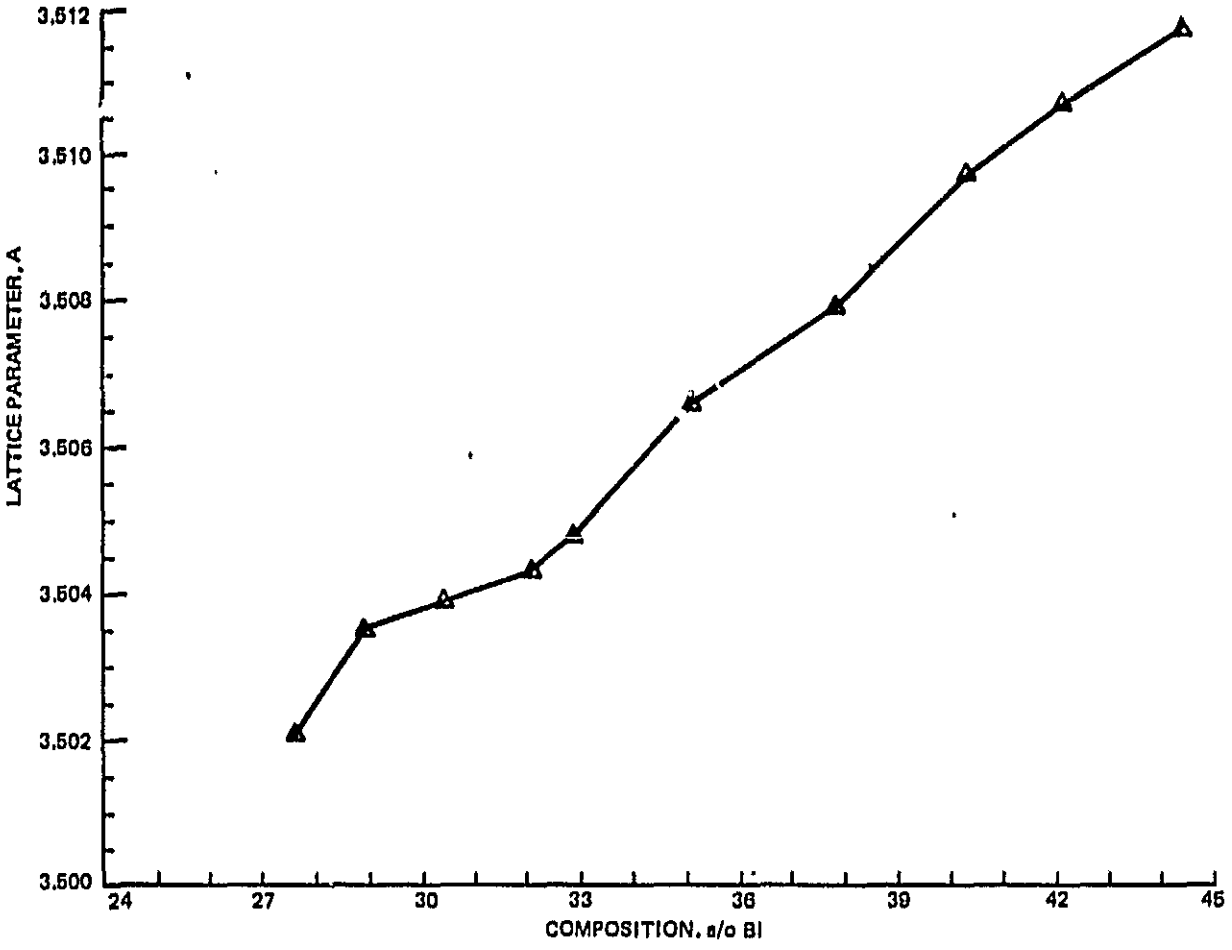

1875-021A

Fig. 21 Lattice Parameter, a, of PbBi Peritectic Phase, β, as a Function of Bi Concentration (Sheet 1 of 2)

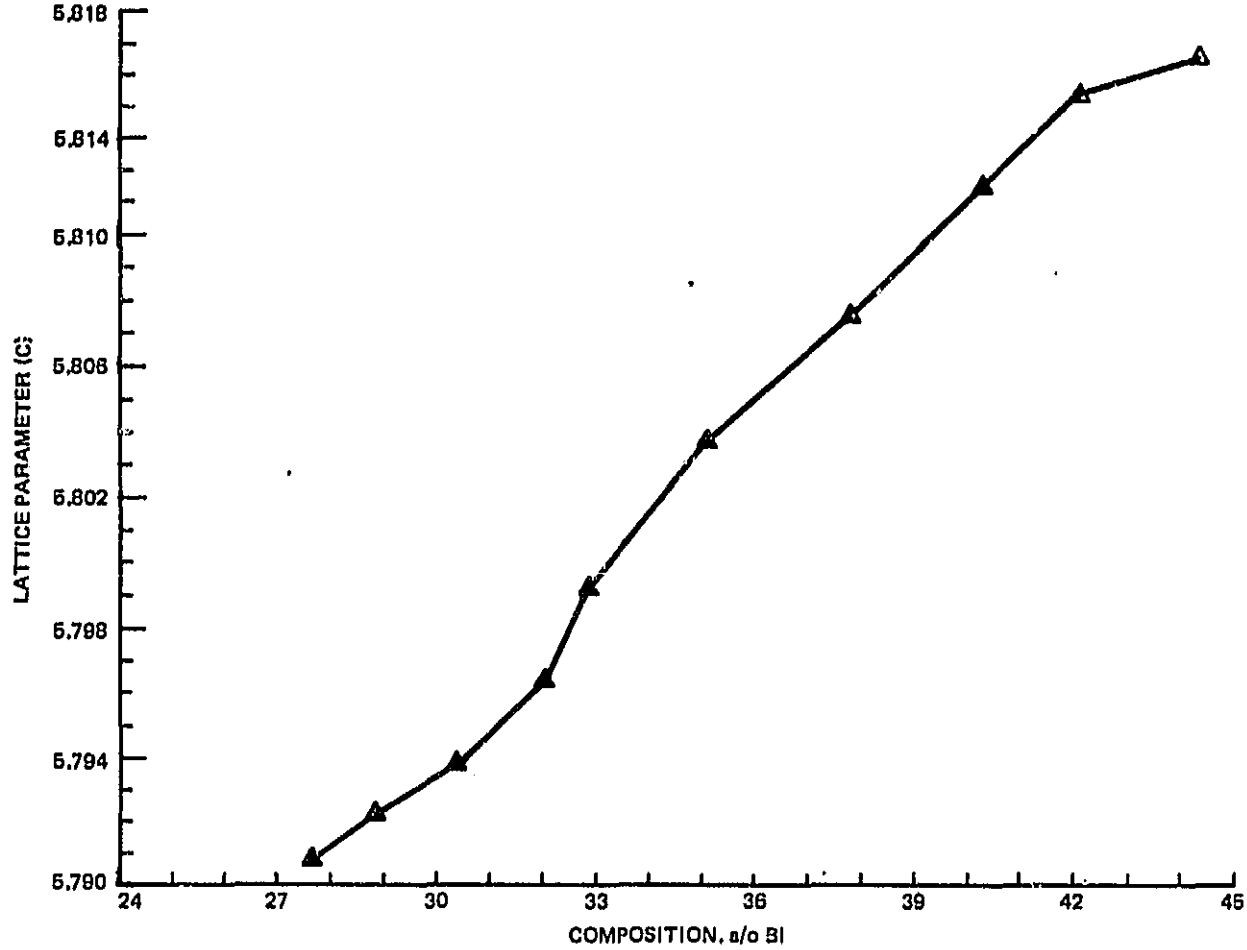

Fig. 21 Lattice Parameter, C, of PbBi Peritectic Phase, β, as a Function of Bi Concentration (Sheet 2 of 2)

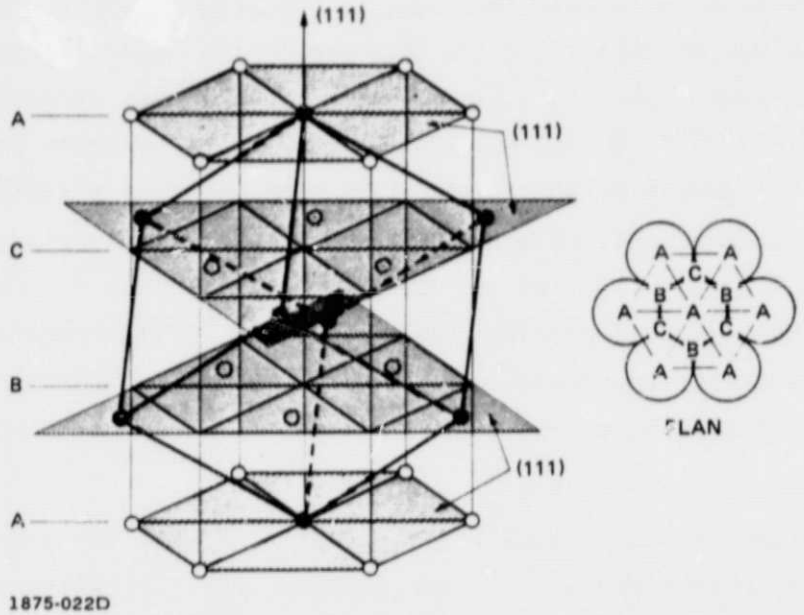

Fig. 22 Face-Centered Cubic/Hexagonal Close-Packed Crystallographic Relationships

The terminal solid solution Bi phase, ε, is rhombohedral (R). A possible crystallographic relationship between the HCP β phase, and the R phase is shown in Fig. 23 (Ref. 19). For this example the [0001] HCP direction is coincident with the [111] R direction and the (0003) HCP basal plane is parallel to the $(11_{\bar{1}})$ R plane. The solidification system for rhombohedral systems is usually in the 'C' direction, [111] R, on the prism planes (110) R.

If x-ray analyses are conducted on longitudinal sample sections polished parallel to the solidification direction, then the reflecting planes detected offer strong evidence as to the solidification sequence. For instance, if a primary α single crystal were to grow, with a [100] growth direction, then all of the theoretically allowable FCC diffraction peaks might be detected for a longitudinal plane of polish and the β phase, which would precipitate during the cooling to room temperature, would diffract from all reflecting planes, including (000n)β. If, on the other hand, β were the primary phase solidifying, the growth direction would be parallel to the [0001]β direction and a similar plane of polish would not detect the (000n)β planes. Similarly, if metastable β were solidified and decomposed during the cooling to room temperature, then α would precipitate from the β. If the anticipated β growth system and α+β crystallographic relationship held, then neither the (000n) HCP planes nor the (111) FCC planes should be seen for a longitudinal plane of polish.

The important point to note here, however, is that the coexistence of phases, or the absence thereof, in conjunction with crystallographic orientation relationships, and the presence of diffraction planes or the absence thereof, can contribute significantly to the understanding of the solidification sequence.

Directionally solidified samples, then, were longitudinally polished and the discrete morphological regions were investigated using standard x-ray goniometer techniques. The objectives of this effort were to address the crystallography of the solidification sequence, the interphase crystallographic relationships of the α and β phases, and by correlation with reference literature, the composition of phases within these morphological regions.

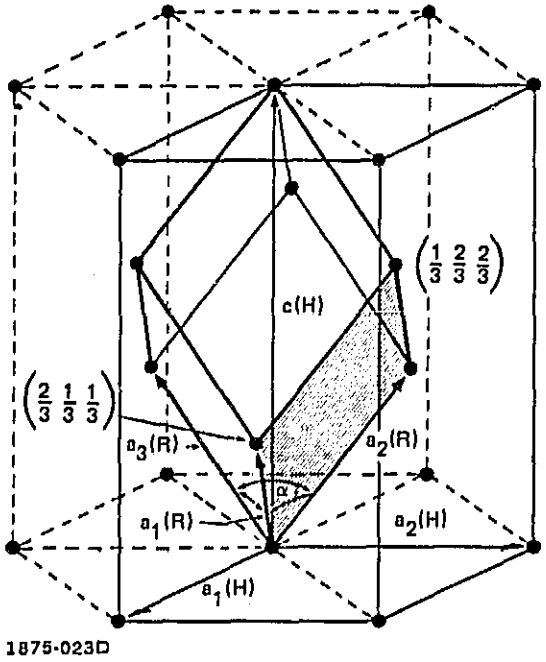

Fig. 23 Rhombohedral & Hexagonal Unit Cells in a Rhombohedral Lattice

The macrochemical distribution and the discrete morphological regions of interest for a typical directionally solidified 30 w/o Bi sample are shown in Fig. 24. This distribution was typical of samples solidified under plane front conditions at velocities of 2 mm/hr. The macrosegregation is evident, as previously noted, however it is less severe than the distributions noted last year. It was concluded that the reduced radial gradients substantially reduced the driving force for buoyancy driven convection which in turn reduced the severity of the macrosegregation. Each longitudinal region was analyzed, by x-ray diffraction and, if additional information was needed, also transversely.

The properitectic α region consists of two phases, terminal solid solution α and dispersed β which has precipitated from the supersaturated solid solution on cooling. The lattice parameters of these phases were determined using the Nelson-Riley method and the results for all of the samples monitored are summarized in Table 1. Table 2 summarizes the same data, but as the compositional equivalent of the phases using the data of Figs. 20 and 21. It is clear from Tables 1 and 2 that there is a consistency in these data sets and that the average α composition is 18 ± 1 w/o Bi whereas the average β composition is 29 ± 2 w/o Bi in good agreement with the phase diagram. The wider spread in the β phase composition data is in part due to the fact that β compositions formed at all temperatures are stable to room temperature, whereas α compositions will continuously adjust to the composition at the lowest temperature at which sufficient solid state diffusion occurs. The precipitated β thus exists in a range of compositions whereas the α composition tends to be singular. Another uncertainty in the β values relates to the c/a ratio selected during the fitting operation. Table 3 presents the crystallographic reflecting planes from a typical properitectic region and illustrates that the number of reflecting planes analyzed was large, resulting in a good fit. Crystallographically, the (000n) β and $(10\bar{1}n)\beta$ families of planes are dominant for the β phase. This orientation relationship with the parent α phase was inconsistent with the plane of polish and the solidification growth habit for β, but entirely consistent with a solid state parent/product precipitation of β within α. As a consequence it was concluded that plane front proeutectic α solidified in this region and β subsequently precipitated in the solid state during cooling or even while stored at room temperature.

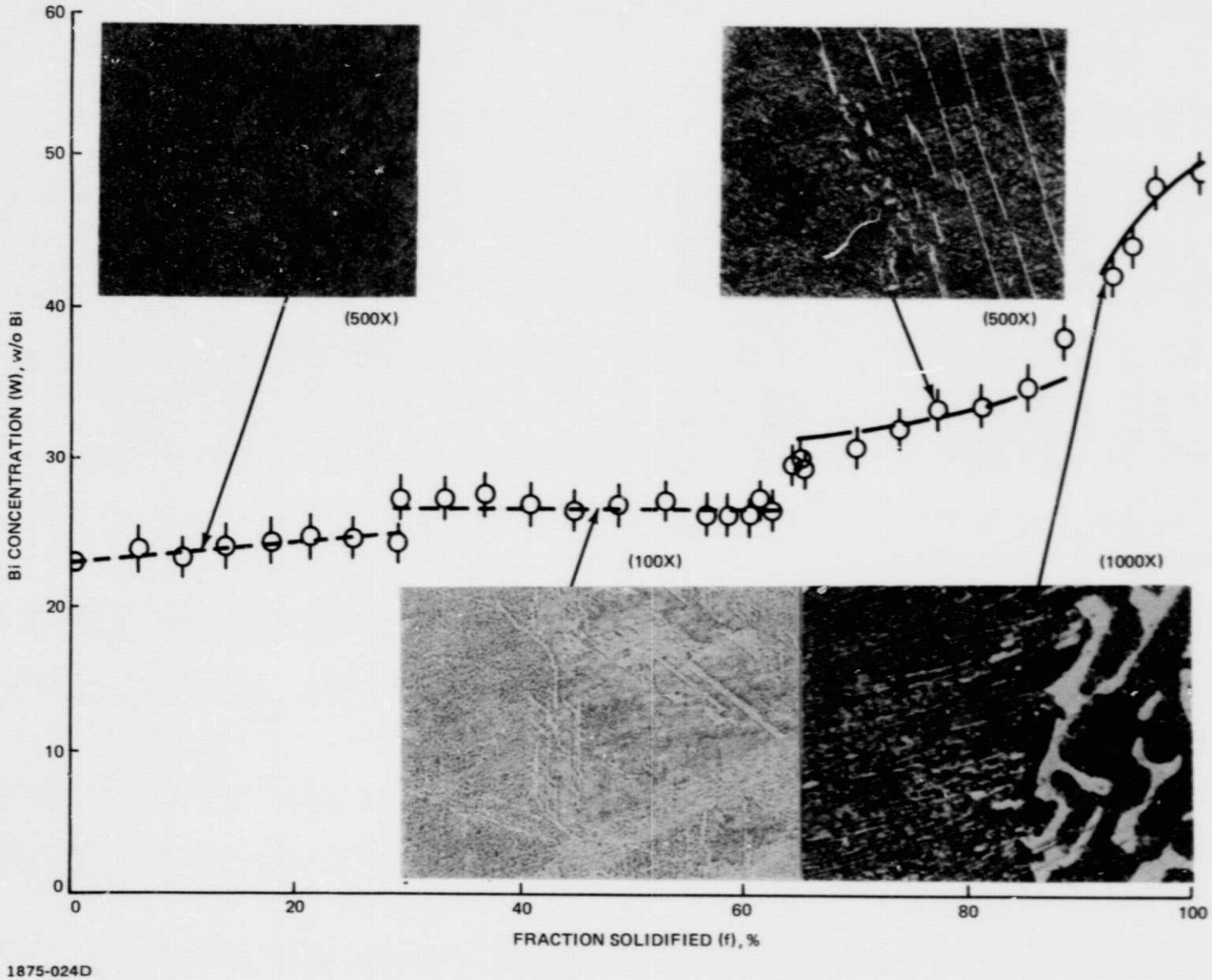

1875-024D

Fig. 24 Sample Composition vs Fraction Solidified, for Pb-30 w/o Bi Alloy With Superimposed Micrographs of Morphologically Distinct Regions

Table 1. Summary of Lattice Parameter Data For the α and β Phases Within The Properitectic Morphological Region of Directionally Solidified Pb-28 w/o Bi Alloys

SAMPLE	ALPHA a_o(FCC), Å	BETA a(HCP)	c(HCP)
Q7	4.9731 ±0.0007	3.5033 ±0.0011	5.7910 ±0.0019
Q8	4.9719 ±0.0011	3.5064 ±0.0019	5.7943 ±0.0031
Q9	4.9716 ±0.0008	-	-
Q10	4.9712	-	-
Q11	4.9731 ±0.0003	3.5072 ±0.0009	5.7939 ±0.0015
Q12	4.9734 ±0.0009	3.5063 ±0.0031	5.7942 ±0.0050

Table 2. Summary of Compositional Equivalents of Lattice Parameter Data Shown In Table 1

SAMPLE	ALPHA w/o Bi	BETA w/o Bi
Q7	20±0.7	28.4±0.4
Q8	18.7±1.1	30.8±0.6
Q9	18.5±0.8	-
Q10	17.0	-
Q11	20±0.3	30.2±0.3
Q12	20.3±0.9	30.6±1.0

Table 3. Diffracting Planes, Intensities, 'd' Spacings, and Intensities Typical of the Properitectic and Hypoperitectic Regions of Directionally Solidified 28 w/o Pb-Bi Alloys.

2θ	I	d Spacing	plane/phase reflecting
27.893	132	2.88818 K_β	(0002) β
28.123	30	2.86503 K_β	(101) α
29.493	57	3.02858 K_α	(10$\bar{1}$0) β
30.092	30	2.68139 K_β	(10$\bar{1}$1) β
31.053	1500	2.87990 K_α	(0002) β
33.393	400	2.68102 Kα1	(10$\bar{1}$1) β
33.452	255	2.68300 Kα2	(10$\bar{1}$1) β
36.173	350	2.48109 Kα1	(200) α
36.223	225	2.48394 Kα2	(200) α
43.213	135	2.09179 Kα1	(10$\bar{1}$2) β
43.313	78	2.09238 Kα2	(10$\bar{1}$2) β
52.022	135	1.75637 Kα1	(220) α
52.192	84	1.75540 Kα2, 1.75104 Kα1	(220) α, (11$\bar{2}$0) β
52.353	45	1.75041 Kα2	(11$\bar{2}$0) β
56.493	267	1.62753 Kα1	(10$\bar{1}$3) β
56.632	147	1.62788 Kα2	(10$\bar{1}$3) β
61.893	207	1.49786 Kα1	(311) α
62.052	108	1.49810 Kα2	(311) α
63.382	42	1.46619 Kα1	(21$\bar{3}$0) β
63.543	18	1.46652 Kα2	(20$\bar{2}$1) β
64.322	450	1.44701 Kα1	(0004) β
64.503	300	1.44700 Kα2	(0004) β
64.943	90	1.43469 Kα1	(222) α
65.122	48	1.43472 Kα2	(222) α
69.982	18	1.34318 Kα1	(20$\bar{2}$2) β
72.262	48	1.30631 Kα1	(10$\bar{1}$4) β
72.492	21	1.30597 Kα2	(10$\bar{1}$4) β
80.482	30	1.19232 Kα1	(20$\bar{2}$3) β
80.723	21	1.19234 Kα2	(20$\bar{2}$3) β
84.952	33	1.14063 Kα1	(331) α
85.212	21	1.14064 Kα2	(331) α
86.473	21	1.12444 Kα1	(21$\bar{3}$1) β
87.313	33	1.11577 Kα1	(11$\bar{2}$4) β
87.712	36	1.11171 Kα1	((420) α
87.982	24	1.11175 Kα2	(420) α
90.753	72	1.08221 Kα1	(10$\bar{1}$5) β
91.042	36	1.08221 Kα2	(10$\bar{1}$5) β
98.753	27	1.01482 Kα1	(422) α
99.023	21	1.01529 Kα2	(422) α
102.813	21	0.98549 Kα1	(21$\bar{3}$3) β
103.163	12	0.98555 Kα2	(21$\bar{3}$3) β
105.822	75	0.96559 Kα1	(0006) β
106.283	36	0.96507 Kα2	(0006) β
107.232	33	0.95676 Kα1	(33$\bar{6}$3) β
107.613	27	0.95680 Kα2	(33$\bar{6}$3) β
132.783	21	0.84061 Kα1	(53$\bar{2}$1) β
136.638	21	0.82889 Kα1	(600) β

The peritectic β phase forms as a morphologically distinct region that showed no high angle grain boundaries metallographically, as was the case with the properitectic α phase. This indicated that under the imposed thermal conditions essentially single crystal growth of PbBi, β, had occurred. X-ray diffraction of longitudinal sections of the β region showed entirely single phase behavior in the first regions of β solidification with a crystallographic orientation such that the (000n) planes were not detected for a longitudinal plane of polish, as shown in Table 4. This is consistent with the usual solidification habit of HCP phases and supports, in concert with the metallographic data, the single crystal growth of HCP, β. It should be emphasized that the absence of the (000n) planes is dramatic since these were dominant peaks in the properitectic regions of the sample.

As the Bi content of the peritectic β phase increases, rhombohedral ε begins to precipitate in the solid state during cooling. This was discussed in Section 3.2 Morphological Transitions. Whereas the crystallographic interrelationships between the β and ε phases might have been further explored from the body of x-ray data available, they were not because this was not the focus of this study. Similarly, as the off-eutectic and eutectic regions were analyzed, only phase identification aspects were pursued. In these regions, and also in the regions of β+ε quenched liquid, no metastable phase formation was noted.

The most important region, and the focal point of this study, was the morphological region that we have previously described as twinned or cellular. This region appears in Fig. 24 to be compositionally in the α + β two phase equilibrium phase field and seems to be nearly isocompositional. Some samples indicated a weakly increasing composition with fraction solidified in this region and in all cases the 'step' in the composition which is shown in Fig. 24 was within the error bars of the determination, possibly indicating a solidification process continuous with the properitectic α.

X-ray analysis of longitudinal sections encompassing these regions, whether twinned or cellular, showed a diffraction spectra consistent with the

Table 4. Diffracting Planes, Intensities, 'd' Spacings, and Intensities Typical of the Hyperperitectic Regions of Directionally Solidified 28 w/o Pb-Bi Alloys

2θ	I	d Spacing	plane/phase reflecting
26.530	123	3.03364	$(10\bar{1}0)\,\beta$
29.440	3,250	3.03386	$(10\bar{1}0)\,\beta$
33.360	102	2.68355	$(10\bar{1}1)\,\beta$
43.250	15	2.09006	$(10\bar{1}2)\,\beta$
52.200	24	1.75081	$(11\bar{2}0)\,\beta$
52.340	12	1.75080	$(11\bar{2}0)\,\beta$
56.095	81	1.63812	$(10\bar{1}3)\,\beta$
56.235	48	1.63844	$(10\bar{1}3)\,\beta$
61.010	60	1.51739	$(20\bar{2}0)\,\beta$
61.200	42	1.51690	$(20\bar{2}0)\,\beta$
89.660	12	1.09254	$(10\bar{1}5)\,\beta$

properitectic process extended to higher Bi compositions. No regions were identified where primary β solidification was indicated by the crystallographic orientation relationships. Since this region was succeeded by a very discrete morphological and crystallographic transition which involved a substantial crystallographic rotation realigning the β phase, it was concluded that the morphological transition from the α+β to β solidification was discrete (discontinuous) and that properitectic β formation was precluded for the α+β region.

Alternative mechanisms for the formation of the α+β region were evaluated. The two mechanisms examined were metastable extrapolation (supercooling) of the terminal solid solution α solidus to supersaturated (>24 w/o Bi) compositions, or isothermal two-phase hypoperitectic α+β solidification. Crystallographically, these may be indistinguishable in that the crystallographic habit of the β phase growing in concert with the α phase may not be the same as that for β growing independently, and this might account for the presence of (000n)β reflecting planes in sampling orientations that would normally be precluded for primary β solidification.

Since the x-ray results were indeterminate, the compositional data for the quenched interfaces measured by means of an election microprobe were evaluated as a means of differentiating between these possibilities. These data are shown in Fig. 25. Unfortunately, there are large error bars associated with these data; however, the data trend is clear. If the quenched liquid data are plotted (superimposed) on the equilibrium liquidus lines, then the experimental solidus lines indicate that there is a significant solute depletion in each phase, α and β, that the α solidus line extends to the vicinity of 165°C at which temperature there is a discontinuous transition to β phase formation. This result is surprisingly consistent with that of Ref. 11 in which they report that in vacuum β could not nucleate above 167°C. Our ampoules were evacuated.

Quantitatively, these data support a metastable extension of the properitectic α solidus and liquidus lines of about 20°C. However the absolute values of these data, and the error bars, leave a lot to be desired and further quantitative work will have to be conducted. The solute depletion of the properitectic α and hyperperitectic β compositions is readily accounted

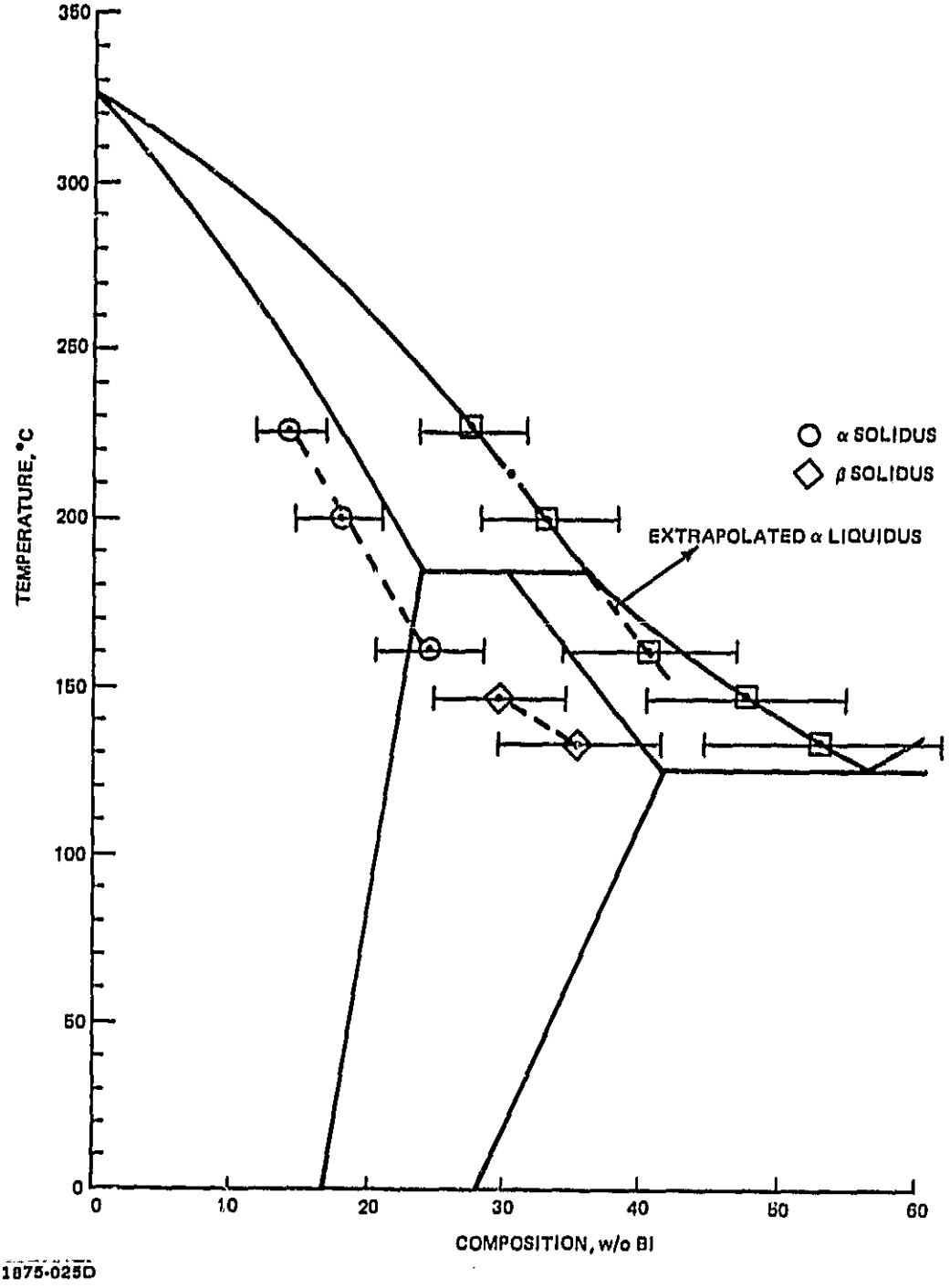

Fig. 25 Interface Quench Results (S/L) Superimposed On The Equilibrium Phase Diagram

for with standard solidification theory whereby an effective redistribution coefficient, k_{eff}, is utilized instead of k_{equ}.

One additional point should be noted. This relates to the diffraction data within the twinned and cellular regimes. As the morphology ages at room temperature from the as-grown twinned structure to the fully developed lamellar structure there is an intensification (depletion) of the β phase (α phase) diffraction peaks which is noticeable. This was interpreted to indicate that as the morphology adjusted, the relative proportion of the phases adjusted also in accordance with a constant bulk composition but a changing lever law relationship at room temperature which would serve to increase the relative proportion of β.

4. SUMMARY

1. Banding is not the characteristic morphology for plane front solidification of two-phase peritectic alloys.

2. No evidence was found which supported the formation of a metastable Pb-rich PbBi phase, β, which formed above the peritectic isotherm.

3. A morphologically distinct region was identified that coincided with plane front solidification within the two-phase peritectic phase field. This region was crystallographically continuous with the properitectic α solidification, was isocompositional within our experimental error and seemed to be formed by a supersaturation/undercooling mechanism. It consisted of a fine dispersion of the β phase within α, but which developed on aging at room temperature into a cellular two-phase α+β mixture. The latter structure was clearly the result of a solid state transformation and was not directly the result of solidification processing.

4. Pb-Bi directional solidification was, once again, shown to be subject to significant macrosegregation under plane front growth conditions which was due, presumably, to gravitationally driven convection.

5. Fine sub-micron dispersions of aligned Bi rods were noted within a parent PbBi matrix. This morphology is thought to be the result of solid state precipitation of Bi, ε, from the supersaturated PbBi, β, while still in a steep thermal gradient.

5. REFERENCES

1. B. Chalmers, Physical Metallurgy, John Wiley & Sons, New York, pp 271-72 1959.

2. D.R. Uhlmann and G.A. Chadwick, Acta Met., Vol 9, pp 835-40 (1961).

3. B. Chalmers, Principles of Solidification, John Wiley & Sons, New York, pp 224-27, 1964.

4. J.D. Livingston, Mat. Sci. Eng, Vol 7, pp 61-70, 1971.

5. M.C. Flemings, Solidification Processing, McGraw-Hill, New York, pp 117, Vol 178, 1974.

6. W.J. Boettinger, Met. Trans, Vol 5, pp 2023-2031, 1974.

7. K.A. Jackson and J.I. Hunt, Trans. TMS-AIME, Vol 236, pp 1129-42, 1966.

8. A.P. Titchener and J.A. Spittle, Acta Met., Vol 23, pp 497-502, 1975.

9. H.W. Kerr, J. Cisse, and G.F. Bolling, Acta Met., Vol 22, pp 677-686, 1974.

10. G.I. Scherbakov, S.A. David, and M.D. Brody, Scripta Met., Vol 8, pp 1239-44 1974.

11. B.W. Sundquist and L.F. Mondolofo, Trans Met Soc AIME, p 157, 1961.

12. D.M. Goddard and W.J. Childs, J. Less Common Metals, Vol 58, pp 217-29 1978.

13. D.J. Larson, Jr, R G. Pirich, and W.R. Wilcox, The Growth Of Metastable Peritectic Compounds, First Annual Report on Contract NAS8-32998, Grumman Research Department Memorandum RM-714, January 1981.

14. B. Predel and W. Schwermann; Z. Metallk., Vol 58, p 553, 1967.

15. J.B. Nelson and D.P. Riley, Proc. Phys. Soc., Vol 57, p 160, 1945.

16. K. Cooper, Thermal Undercooling of PbBi Alloys, Ph.D. Thesis, University of Wisconsin, June, 1981.

17. Ta-Wei Fu and W.R. Wilcox, Journal of Crystal Growth, Vol 51, pp 557-567, 1981.

18. F.M. Carson, Proceedings ofthe Materials Research Society Annual Meeting, November 1981 1981, Boston, Mass. Editor, Guy E. Rindone, North Holland Pbulishing 1982.

19. B.D. Cullity, Elements of X-Ray Diffraction, Addison-Wesley Publishing Company, Inc., 1956.

20. W.P. Pearson, A Handbook of Lattice Spacings and Structures of Metals and Alloys, Pergamon Press, 1958.

6. ACKNOWLEDGEMENTS

The author would like to thank Dr. R.G. Pirich of the Grumman R&D Center for collaboration on this effort. In addition the author is grateful to Dr. P.N. Adler of the Grumman R&D Center, Dr. John Perepezko of the University of Wisconsin at Madison, and Dr. Martin Glicksman of Rensselaer Polytechnic Institute for helpful discussions. Further, the author is indebted to Mr. Garrett Busch, Mr. William Poit, and Mr. Ralph Lange of the Grumman R&D Center for their valuable support. Lastly, the author would like to acknowledge, with thanks, the financial support provided by NASA, Marshall Space Flight Center, under contract NAS-8-32998.